nature cell biology

Control of vertebrate multiciliogenesis by miR-449 through direct repression of the Delta/Notch pathway

Brice Marcet[1,2], Benoît Chevalier[1,2,11], Guillaume Luxardi[3,4,11], Christelle Coraux[5,6,11], Laure-Emmanuelle Zaragosi[1,2], Marie Cibois[3,4], Karine Robbe-Sermesant[1,2], Thomas Jolly[5,6], Bruno Cardinaud[1,2,7,8], Chimène Moreilhon[1,2,9], Lisa Giovannini-Chami[1,2,10], Béatrice Nawrocki-Raby[5,6], Philippe Birembaut[5,6], Rainer Waldmann[1,2], Laurent Kodjabachian[3,4,12] and Pascal Barbry[1,2,12,13]

Multiciliated cells lining the surface of some vertebrate epithelia are essential for various physiological processes, such as airway cleansing[1–3]. However, the mechanisms governing motile cilia biosynthesis remain poorly elucidated. We identify miR-449 microRNAs as evolutionarily conserved key regulators of vertebrate multiciliogenesis. In human airway epithelium and *Xenopus laevis* embryonic epidermis, miR-449 microRNAs strongly accumulated in multiciliated cells. In both models, we show that miR-449 microRNAs promote centriole multiplication and multiciliogenesis by directly repressing the Delta/Notch pathway. We established Notch1 and its ligand Delta-like 1 (DLL1) as miR-449 *bona fide* targets. Human DLL1 and NOTCH1 protein levels were lower in multiciliated cells than in surrounding cells, decreased after miR-449 overexpression and increased after miR-449 inhibition. In frog, miR-449 silencing led to increased *Dll1* expression. Consistently, overexpression of *Dll1* mRNA lacking miR-449 target sites repressed multiciliogenesis, whereas both *Dll1* and *Notch1* knockdown rescued multiciliogenesis in miR-449-deficient cells. Antisense-mediated protection of miR-449-binding sites of endogenous human *Notch1* or frog *Dll1* strongly repressed multiciliogenesis. Our results unravel a conserved mechanism whereby Notch signalling must undergo miR-449-mediated inhibition to permit differentiation of ciliated cell progenitors.

Motile cilia are microtubule-based organelles that develop from the apical surface of specialized cells in varying numbers, ranging from one to several hundred per cell[1,2]. They have important mechanical and sensory roles[1,2], highlighted by the fact that a wide variety of human pathologies, such as chronic airway diseases (including primary ciliary dyskinesia, cystic fibrosis and chronic obstructive pulmonary disease), Bardet–Biedl syndrome and reproductive disorders[1,2], are associated with ciliary defects. Multiciliated epithelia are morphologically conserved among vertebrates, indicating that the key pathways that control multiciliogenesis are also conserved across this phylum[1,2,4–6]. We formed a hypothesis that microRNAs, a class of small regulatory noncoding RNAs (refs 7–9), may be important regulators of vertebrate multiciliogenesis. To test our hypothesis, we examined the microRNA expression changes during ciliogenesis in two models derived from evolutionarily distant tetrapods: primary cultures of differentiated human airway mucociliary epithelial cells (HAECs) grown at an air–liquid interface[10–12] (Supplementary Fig S1a,b), and mucociliary epidermis of *Xenopus* embryos[4,6]. Both models recapitulate the different steps leading to terminal differentiation into multiciliated cells, characterized by the growth of hundreds of motile cilia at the apical surface of each cell. For HAEC primary cultures, we established microRNA signatures by high-throughput sequencing (HTS) at four characteristic time points of the airway barrier regeneration: proliferation, immediately after the establishment of an air–liquid interface (ALI-D0); polarization, which was typically observed after 7 days (ALI-D7); onset of ciliogenesis, after 14 days (ALI-D14); and terminal differentiation, after 21 days (ALI-D21). For *Xenopus laevis*, we sequenced microRNAs from ectoderm explants at stage 11.5 (gastrula), which is before the appearance of multiciliated cells, and at stage 26 (tailbud), when the ciliated epidermis is fully developed. miR-449a, miR-449b and miR-449c (collectively named miR-449), constitute by far the most strongly induced microRNAs during epithelium differentiation in both species. Although representing less than 0.01% of all microRNA sequences in proliferating HAECs, miR-449 accounted for more than 8% of the microRNA reads in

[1]CNRS, Institut de Pharmacologie Moléculaire et Cellulaire, F06560 Sophia Antipolis, France. [2]University of Nice-Sophia-Antipolis, F06560 Sophia Antipolis, France. [3]CNRS, Institut de Biologie du Développement de Marseille-Luminy, F13288 Marseille, France. [4]University of Méditerranée, F13288 Marseille, France. [5]INSERM, U903, F51092 Reims, France. [6]University of Reims Champagne-Ardenne, F51092 Reims, France. [7]INSERM, U876, F33076 Bordeaux, France. [8]University of Bordeaux 2, F33076 Bordeaux, France. [9]CHU de Nice, Service d'Hématologie-Biologie, Hôpital Pasteur, F06000 Nice, France. [10]CHU de Nice, Service de Pédiatrie, Hôpital l'Archet 2, F06200 Nice, France. [11]These authors contributed equally to this work. [12]Co-senior authors.
[13]Correspondence should be addressed to P.B. (e-mail: barbry@ipmc.cnrs.fr)

Received 20 December 2010; accepted 24 March 2011; published online 22 May 2011; DOI: 10.1038/ncb2241

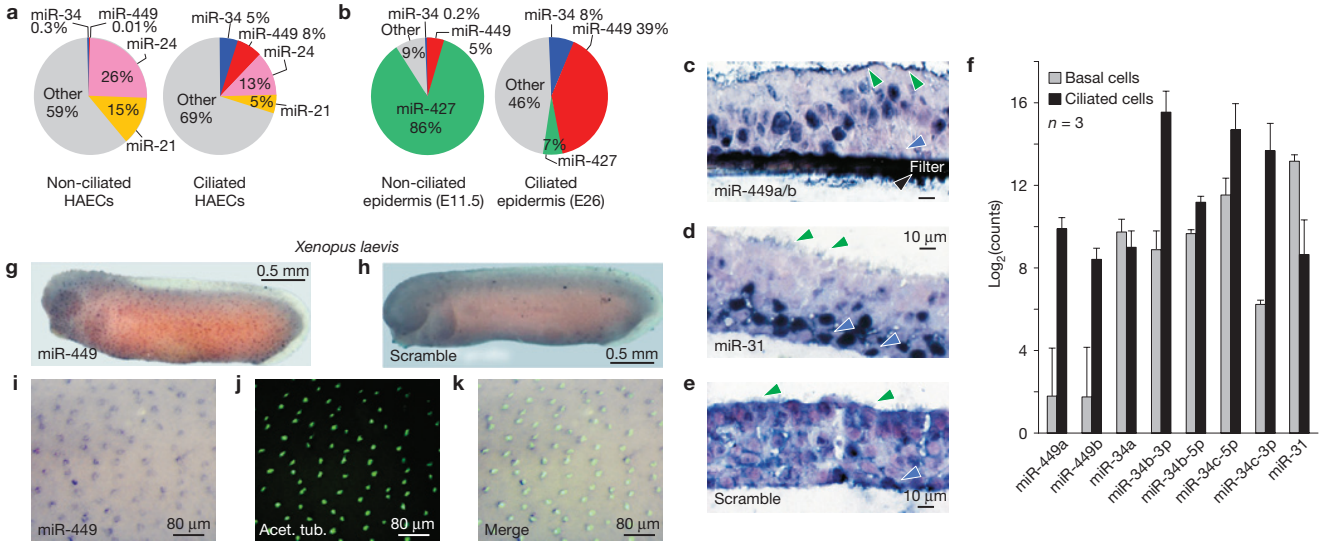

Figure 1 miR-449 microRNAs are the most upregulated microRNAs during multiciliogenesis. (**a**,**b**) Pie charts illustrating the relative microRNA abundance (percentage of microRNA reads) in undifferentiated (non-ciliated; ALI-D0) versus differentiated (ciliated; ALI-D21) HAEC cultures (**a**) and in *Xenopus* epidermal explants from embryos before (E11.5) and after (E26) the onset of multiciliogenesis (**b**; see also Supplementary Fig. S1). The miR-449 and miR-34 families are indicated in red and blue, respectively. Data are from HTS ($n = 3$ donors). Similar results were obtained with microarrays ($n = 3$ donors; Supplementary Fig. S1f). (**c**–**k**) Specific localization of miR-449 in multiciliated cells. *In situ* hybridization was carried out on frozen sections of 21-day ALI cultures (**c**–**e**) or from tailbud embryos of *Xenopus* (**g**–**k**) with digoxigenin-labelled LNA probes against miR-449 (**c**,**g**,**i**,**k**), miR-31 (**d**) and scrambled probes as a negative control (**e**,**h**). *In situ* hybridization results are representative of three individual experiments. In human (**c**–**e**), cross-sections of a well-differentiated pseudostratified epithelium revealed layers of nuclei located at different heights: a first layer is near the permeable support and corresponds to basal cells. This layer was miR-31-positive (**d**). A second layer is located in the middle of the section, and corresponds to columnar cells. It was miR-449-positive (**c**). Cilia of multiciliated cells are indicated on the panels by green arrowheads, basal cells by blue arrowheads, and no mucus-secretory cells are morphologically detectable in those images (**c**–**e**). The dark zone at the base of the tissue indicated by a black arrowhead in **c** corresponds to the filter used to culture HAECs. Multiciliated cells in *Xenopus* embryos were identified by acetylated-tubulin immunostaining (**j**,**k**). (**f**) HTS expression profiling of miR-449, miR-34 and miR-31 expression levels in FACS-sorted human airway epithelial basal and columnar multiciliated cells (expressed as $\log_2$(counts)). Data are means ± s.d. from three independent experiments. Human airway epithelial basal and columnar ciliated cells were FACS-sorted using two specific markers of the basal cells (CD151 and tissue factor)[20]. We collected $2.87 \pm 0.76 \times 10^6$ $CD151^+/TF^+$ cells (basal cells, at a purity of $97.1 \pm 2.3\%$) and $0.19 \pm 0.05 \times 10^6$ $CD151^-/TF^-$ cells (columnar cells, at a purity of $92.4 \pm 3.3\%$).

differentiated HAECs (Fig. 1a and Supplementary Fig. S1c,d). Similarly, *Xenopus laevis* miR-449a robustly increased over differentiation, representing up to 39% of all microRNA sequences in ciliated epidermal explants (Fig. 1b and Supplementary Fig. S1e). Consistent observations were made in microarray analyses and quantitative PCR assays (see Methods and Supplementary Fig. S1f,g). miR-34 family members were also induced during differentiation in both models (Fig. 1 and Supplementary Fig. S1c–g), although to a lesser extent than miR-449. Interestingly, miR-449 and miR-34 belong to a superfamily of microRNAs sharing a significant identity, including in the 'seed' region that plays a crucial role in target recognition[13,14]. The miR-449 family seems to be conserved through vertebrates: examination of loci syntenic to *Cdc20b* (which hosts the *miR-449* cluster in human and frog) revealed the existence of *miR-449* in all of the completely assembled and in some of the preliminarily assembled or partially sequenced vertebrate genomes that we examined using *in silico* approaches[15,16] (Supplementary Fig. S2 and Table S1).

Differentiated HAECs and frog ciliated epidermis are constituted of different cell types, including mucus-secreting cells and multiciliated cells, as well as basal cells in HAECs and ionocytes in *Xenopus*[4]. Multiciliogenesis sequentially involves permanent exit from the cell cycle; centriologenesis, characterized by the production of hundreds of basal bodies, made up from neo-synthesized centrioles; and basal body migration to the apical membrane, where they act as microtubule-organizing centres and allow the assembly of motile axonemes[1,5,17–19]. Several lines of evidence indicate that in both species, miR-449 microRNAs are significantly enriched in multiciliated cells. First, *in situ* hybridization of HAEC primary cultures (Fig. 1c–e) and of human bronchial tissue (Fig. 2a–c) detected miR-449 mainly in columnar multiciliated cells but not in basal cells (Fig. 1c), or in muc5AC-positive secretory cells (Fig. 2a). Second, miR-449 microRNAs were preferentially detected in β4-tubulin-positive multiciliated cells in cytospins of HAECs ($P < 0.001$; Fig. 2d–g). Third, immunostaining experiments revealed that CDC20B (cell division cycle 20 homologue B), the protein encoded by the host gene of miR-449, co-localized with centrin-2, a marker of basal bodies in multiciliated cells, but not with muc5AC, a marker of goblet cells (Fig. 2h–m). Fourth, microRNA profiling of columnar cells (mainly composed of multiciliated cells and few mucus-secreting cells) and of basal cells obtained after fluorescence-activated cell sorting (FACS) of HAECs (ref. 20) showed that miR-449 expression was more than two orders of magnitude higher in multiciliated cells than in basal cells, whereas the opposite distribution was observed for miR-31 (Fig. 1f). Fifth, in *Xenopus* embryonic epidermis (Fig. 1g–k) and nephrostomes (Supplementary Fig. S3b), miR-449 expression was also prominent in multiciliated cells that were positive for acetylated tubulin. Epidermal miR-449 was first detected in a 'salt and pepper' pattern at the early neurula stage, indicating that miR-449 microRNAs accumulate in ciliated

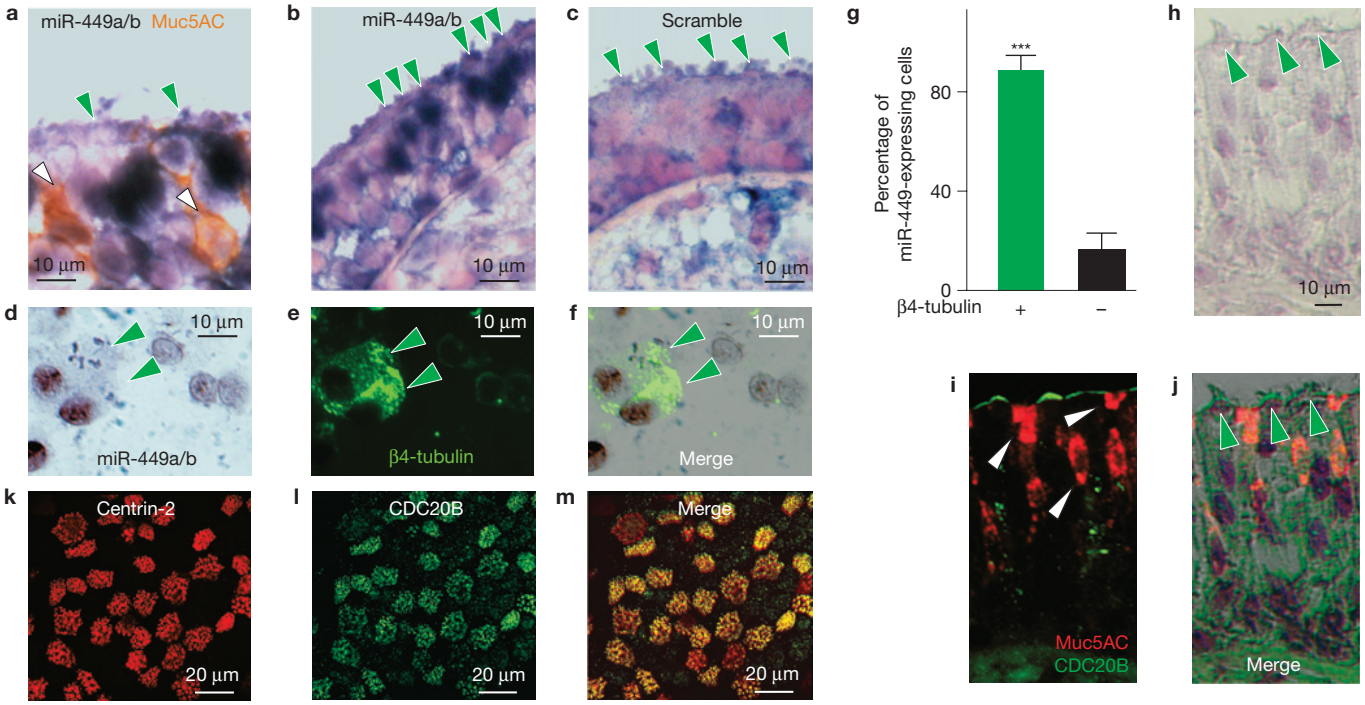

Figure 2 miR-449 and CDC20B are localized in multiciliated cells of human airway epithelium. (**a**–**c**) *In situ* hybridization on frozen sections from human bronchial tissue sections using a digoxigenin-labelled LNA probe against miR-449a/b (**a**,**b**) or a scrambled probe as a negative control (**c**). Green arrowheads indicate multiciliated cells. White arrowheads indicate mucus-secreting cells labelled using anti-Muc5AC antibodies. (**d**–**f**) *In situ* hybridization on cytospins of freshly isolated HAECs ($n = 3$ donors) using a digoxigenin-labelled LNA probe against miR-449a/b (**d**,**f**), and anti-4-tubulin antibody to label multiciliated cells (green; **e**,**f**). Green arrowheads indicate multiciliated cells. (**g**) Cells stained as in **d**–**f** were assessed for miR-449a/b staining. Multiciliated cells were significantly positive for miR-449a/b (***, $P < 0.001$, Student's *t*-test; 15 fields per slide, three slides per donor, $n = 3$ donors). Data are means ± s.e.m. (**h**–**m**) Immunocytochemistry experiments were carried out on human bronchial tissue sections (**h**–**j**) or on primary cultures of differentiated HAECs at ALI-D21 ($n = 3$ donors; **k**–**m**). (**i**,**j**,**l**,**m**) CDC20B antibody was used to identify cells expressing miR-449 (green), which is located in intron 2 of the *Cdc20b* gene. CDC20B co-localized with multiciliated cells (multiciliated cells indicated by green arrowheads in **h**,**j** and by centrin-2 staining for basal bodies in **k**,**m**), whereas CDC20B did not co-localize with muc5AC-positive cells (red in **i** and indicated by white arrowheads). Gene expression studies have revealed that in HAECs the miR-449/*cdc20b* locus delivers, in a coordinated manner, *cdc20b* transcripts and miR-449 copies.

cell progenitors (CCPs) before the onset of terminal differentiation (Supplementary Fig. S3a). Collectively, our data reveal a robust enrichment of miR-449 expression in vertebrate multiciliated cells.

To investigate the function of miR-449 in multiciliogenesis, six independent HAEC cultures were transfected with a cholesterol-conjugated antagomiR directed against miR-449a/b (AntagomiR-449a/b) and ciliogenesis was assessed over the time course of regeneration. The antagomiR specifically knocked down miR-449 expression (Fig. 3b) and led to a significant reduction in the number of β4-tubulin-positive cells at ALI-D21 (average of ciliogenesis inhibition: 2.3 ± 0.3-fold, $n = 6, P < 0.001$; Fig. 3a). We also knocked down miR-449 in *Xenopus* embryos by epidermal injection of a cocktail of morpholino antisense oligonucleotides targeting mature miR-449a/b/c. miR-449 morpholino oligonucleotides strongly repressed multiciliogenesis, as revealed by acetylated-tubulin staining at tailbud and tadpole stages ($n = 112$; Fig. 3g–i and Supplementary Fig. S4a,b). Multiciliogenesis was also impaired in nephrostomes after miR-449 knockdown (Supplementary Fig. S3c,d). Although miR-449 depletion in *Xenopus* embryonic epidermis inhibited multiciliogenesis, it did not suppress the expression of genes encoding ciliated cell markers, such as α-*tubulin*, *Tex15* (testis expressed 15) and the forkhead transcription factor gene *Foxj1* (Fig. 3c–f and Supplementary Fig. S4a–c), and did not prevent intercalation of CCPs in the outer epidermal layer (Supplementary Fig. S4b). This indicates that miR-449 microRNAs are required for terminal differentiation, but not for specification, of *Xenopus* CCPs. miR-449 inhibition apparently did not affect cell viability in HAECs nor in frog embryos (Supplementary Fig. S4d,e). In both HAECs and *Xenopus* embryonic epidermis, miR-449 knockdown caused a concomitant reduction in the number of cells positive for both tubulin (motile cilia marker) and centrin-2 (basal body marker), indicating that miR-449 microRNAs are required for multiciliogenesis at an early stage of differentiation, before centriologenesis (Supplementary Fig. S5). Our data establish miR-449 microRNAs as key regulators of multiciliogenesis in vertebrates.

Next we investigated how miR-449 microRNAs affect multiciliogenesis. We reasoned that *ad hoc* targets of miR-449 should be downregulated during terminal differentiation and after transfection of miR-449. To define miR-449 targets, we analysed the following transcriptional profiles: four time points of HAEC differentiation (ALI-D0, ALI-D7, ALI-D14, ALI-D21) as well as that of; proliferating HAECs transfected with miR-449. Functional annotation of differentially expressed mRNAs with gene set enrichment analysis revealed a significant enrichment in genes associated with G2/M checkpoint regulation and ciliogenesis (Supplementary Fig. S6a). miR-449-modulated transcripts were then analysed with several microRNA target prediction tools[21],

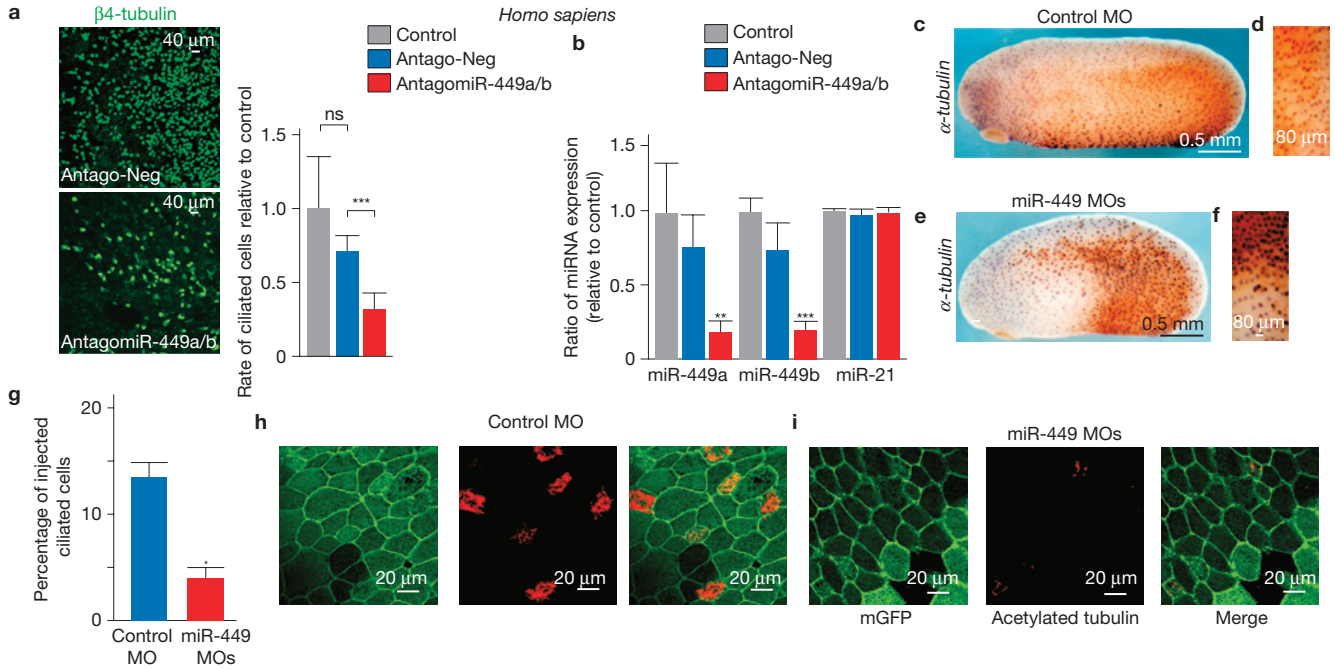

Figure 3 miR-449 knockdown inhibits multiciliogenesis. (**a**,**b**) HAECs ($n = 6$ donors) were chronically treated with anti-miR-449a/b or control antagomiR (20 nM) during the time of differentiation, typically for 21 days at an air–liquid interface. (**a**) Typical β4-tubulin immunostaining of HAECs treated with a negative control antagomiR (Antago-Neg) and an anti-miR-449a/b antagomiR (AntagomiR-449a/b). The relative rate of multiciliated cells was defined as the ratio of the number of β4-tubulin-positive cells to the number of nuclei (20 fields per filter, and 3 inserts per donor, $n = 6$ donors). The histogram indicates the relative rate of multiciliated cells per field in each experimental condition, with the control set to 1. Data are means ± s.d. from six donors (***, $P < 0.001$, Student's t-test). (**b**) Real-time RT–PCR experiments indicate that antagomiR-449a/b inhibits miR-449a and miR-449b expression and has no effect on the unrelated microRNA miR-21. Data are means ± s.d. from six donors (ns, not significant, **, $P < 0.01$, ***, $P < 0.001$, Student's t-test). (**c**–**i**) *Xenopus* cleavage-stage embryos were injected in the epidermis with a mixture of 30 ng control morpholino oligonucleotides (MOs; **c**,**d**,**h**) or miR-449a/b/c morpholino oligonucleotides (10 ng each) and 2.5 ng of FLDx (stained in orange/brown in **c**–**f**) or 500 pg mGFP–CAAX mRNA to stain plasma membranes of injected cells (**g**–**i**). (**c**–**f**) Detection of CCPs by α-tubulin *in situ* hybridization staining. (**f**) The miR-449-depleted region in brown shows an excess of cells positive for α-tubulin transcript when compared with the non-injected region. (**g**) Percentage of injected cells (positive for mGFP green fluorescence) that develop cilia in controls (1,002 cells) and in miR-449 morphants (777 cells, $P = 0.036$, Kruskall–Wallis test). (**h**,**i**) Cilia detection in tailbud stage embryos with an antibody against acetylated tubulin. mGFP immunostaining was used to reveal plasma membranes. miR-449 morphant cells do not exhibit cilia staining.

leading to the identification of several potential targets, which we validated with a dual luciferase assay. A first group of miR-449 targets code for proteins involved in cell cycle regulation (amphiregulin[22], cyclin B1, cyclin E2, and cell division cycle 25 homologue A) that were partially reported elsewhere[23–25] (Supplementary Fig. S7a–d). This is consistent with the capacity of miR-449 to block the cell cycle in proliferating human A549 cells (Supplementary Fig. S7e). Although cell cycle exit is important for commitment towards centriologenesis, a lack of miR-449 in confluent HAECs was not sufficient to restart the cell cycle (not shown). This indicates that once the differentiation program has started, the influence of miR-449 on cell cycle regulation is marginal. We then identified and validated a second group of miR-449 targets associated with proliferation/differentiation, which includes NOTCH1 and its ligand DLL1 (Fig. 4a,b and Supplementary Fig. S7a,b). This prompted us to further examine the role of miR-449-mediated modulation of the Notch pathway in multiciliogenesis. *Dll1* and *Notch1* 3′-untranslated regions (3′-UTRs) contain miR-449-binding sites that are conserved between frog and human (Supplementary Fig. S6b). Mutation of one out of two predicted miR-449-binding sites in the human *Notch1* 3′-UTR, or of two out of three sites in the human *Dll1* 3′-UTR, was sufficient to abrogate the effects of miR-449 in luciferase assays (Fig. 4a). These data indicate that both *Dll1* and *Notch1* are *bona fide* targets of miR-449. Next, we examined whether endogenous NOTCH1 and DLL1 in HAECs are also targeted by miR-449. DNA microarrays, real-time PCR with reverse transcription (RT–PCR) and western blot experiments revealed that miR-449 overexpression reduced the expression of both DLL1 and NOTCH1 in proliferating HAECs (Fig. 4b and Supplementary Fig. S7b), and that miR-449 invalidation increased the expression of both DLL1 and NOTCH1 in differentiating HAECs (Fig. 4b). Consistent with silencing of *Dll1* and *Notch1* expression by miR-449, we detected low levels of both DLL1 and NOTCH1 proteins in multiciliated cells when compared with undifferentiated (data not shown) or with non-ciliated differentiated cells (Fig. 4c–e). Finally, the functional impact of Notch pathway repression by miR-449 was assessed in HAECs through a target protection assay[26] with a cholesterol-conjugated modified oligonucleotide complementary to the conserved miR-449-binding site in the 3′-UTR of human *Notch1*. This protector oligonucleotide strongly repressed the effect of miR-449 in *Notch1* 3′-UTR luciferase assays, and caused an increase in both the *Notch1* transcript level and the number of NOTCH1-positive cells in HAECs (Supplementary Fig. S7f–h). Importantly, *Notch1* protection led to a significant reduction in the number of multiciliated cells, thus phenocopying miR-449 knockdown (Fig. 4f). Conversely,

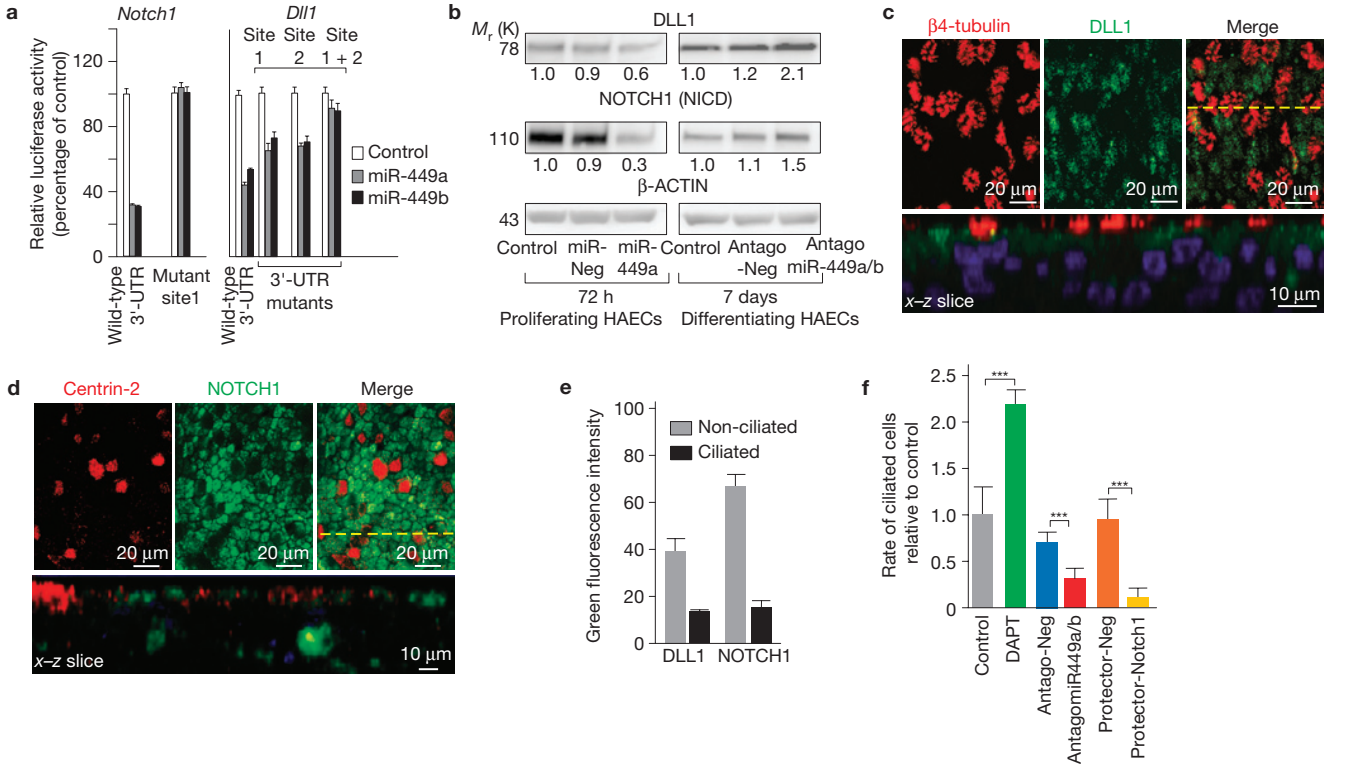

Figure 4 miR-449 microRNAs repress the Notch pathway in HAECs. (**a**) Modulation of the activity of luciferase reporters containing wild-type or mutant 3′-UTRs of human *Dll1* or *Notch1* by miR-449a/b. All experiments were done in triplicate ; $n = 12$ for wild type and $n = 6$ for the mutants. Values were normalized with the internal *Renilla* luciferase control. Error bars denote s.d. (**b**) Modulation of DLL1 and NOTCH1 protein levels by miR-449 overexpression or knockdown with an antagomiR in proliferating and differentiating HAECs. Protein levels were normalized with an antibody against β-actin as an internal control and normalized fold changes are indicated beneath the corresponding bands. Experiments were representative of two donors. (**c**,**d**) In ALI-D21 HAECs, DLL1 and NOTCH1 proteins (in green) were detected primarily in non-ciliated cells as revealed by labelling with β4-tubulin and centrin-2 antibodies, respectively (in red). (**e**) Green fluorescence intensity from experiments performed as in **c**,**d** was quantified by confocal microscopy, thus revealing lower levels of DLL1 and NOTCH1 proteins in multiciliated cells. Data are means ± s.d. from five independent experiments. (**f**) HAECs were chronically treated with antagomiR-449a/b, antago-Neg, Notch1 protector or negative protector oligonucleotides (20 nM) or DAPT (10 μM) for 21 days. The histogram indicates the relative rate of multiciliated cells per field in each experimental condition, with the control set to 1. Data are means ± s.d. $n = 18$, 6, 18, 18, 6 and 6 for control, DAPT, antago-Neg, antago449a/B, protector-Neg, protector-Notch1, respectively. (***, $P < 0.001$, Student's t-test). Uncropped images of blots are shown in Supplementary Fig. S9.

blockade of Notch signalling with a gamma secretase antagonist (DAPT) significantly potentiated multiciliogenesis during HAEC differentiation[27,28] (Fig. 4f). Together, our data indicate that direct repression of the Notch pathway by miR-449 is important for multiciliogenesis in HAECs.

In *Xenopus* epidermis, *Dll1* transcripts are initially present in CCPs, which is thought to permit their specification through Notch-mediated lateral inhibition[29]. However, *Dll1* transcripts are rapidly cleared at the early neurula stage[29], when miR-449 microRNAs become detectable in CCPs. Consistently, we found that inhibition of miR-449 markedly increased the endogenous level of *Dll1* transcripts at the early neurula stage (Fig. 5a). In contrast, we failed to observe any upregulation of *Notch1* transcripts in miR-449 morphant epidermis (data not shown). We thus tested the consequences of sustained DLL1 activity on multiciliogenesis. Injection of a synthetic *Dll1* mRNA devoid of miR-449-binding sites resulted in excessive specification of CCPs (Supplementary Fig. S8a; see also ref. 29), combined with deficient multiciliogenesis (Fig. 5b,c). These effects are identical to those caused by miR-449 depletion (Figs 3g–i and 5b,c). In the converse assay, knockdown of endogenous DLL1 by a translation-blocking morpholino oligonucleotide caused excessive CCP specification but also robust multiciliogenesis (Fig. 5b,c and Supplementary Fig. S8a). Furthermore, the deficient multiciliogenesis caused by miR-449 knockdown was efficiently rescued by silencing *Dll1* (Fig. 5b,c). The widespread derepression of *Dll1* in miR-449-deficient embryos may cause Notch activation across the epidermis, leading to suppression of multiciliogenesis. Consistent with this notion, a morpholino oligonucleotide blocking translation of NOTCH1 also restored multiciliogenesis in miR-449 morphant embryos (Fig. 5b,c and Supplementary Fig. S8a). Finally, two morpholino oligonucleotides complementary to the conserved miR-449-binding sites in the 3′-UTR of *Dll1* (P1P2 morpholino oligonucleotide) were injected to protect *Dll1* from miR-449 binding. As expected, P1P2 protector morpholino oligonucleotides upregulated endogenous *Dll1* transcripts (Supplementary Fig. S8a). Strikingly, these protector morpholino oligonucleotides suppressed multiciliogenesis, but not ciliated cell specification, similarly to miR-449 knockdown and *Dll1* overexpression (Fig. 5b,c and Supplementary Fig. S8a). Our results demonstrate that miR-449-mediated repression of *Dll1* transcripts plays a key role in promoting multiciliogenesis in frog epidermis.

Intriguingly, miR-449 silencing and *Dll1* protection caused enhanced *Dll1* expression in most cells of the epidermis, and increased CCP

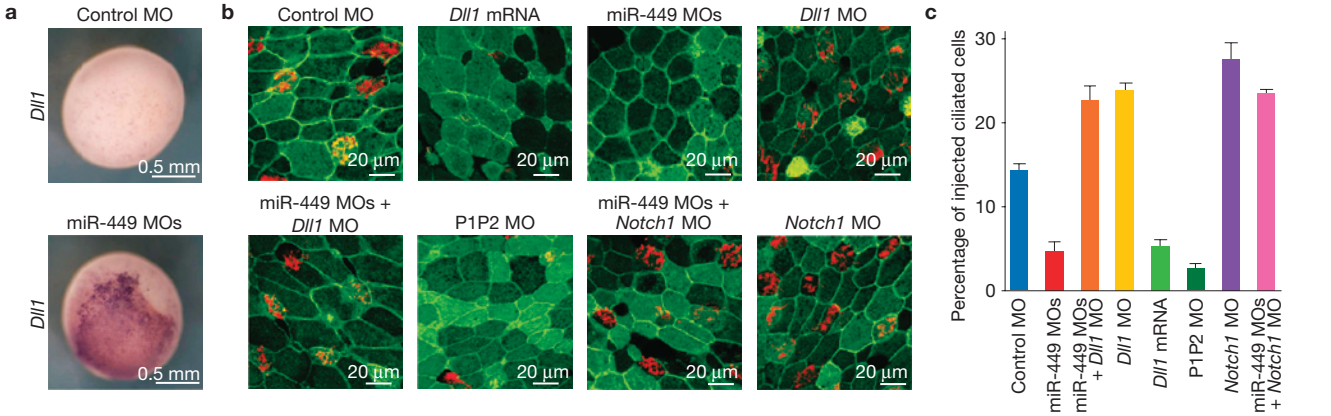

Figure 5 miR-449 microRNAs repress the Notch pathway in *Xenopus* embryonic epidermis. (**a**) Cleavage-stage embryos were injected in the epidermis with a mixture of anti-miR-449 morpholino oligonucleotides (MOs). *In situ* hybridization staining reveals sustained *Dll1* expression in miR-449-deficient epidermis at early neurula stage 14, although the strength and penetrance of this effect was variable between experiments. (**b**) Cleavage-stage embryos were injected in the epidermis with control (50 ng), miR-449 (3 × 10 ng), *Notch1* (20 ng) or *Dll1* (20 ng) morpholino oligonucleotides, *Dll1* mRNA (800 pg) or two morpholino oligonucleotides complementary to the miR-449 target sites in the 3′-UTR of *Dll1* (P1P2 morpholino oligonucleotides, 20 ng each), as indicated. In all cases mGFP–CAAX mRNA was co-injected as a lineage tracer. Co-injection of both miR-449 and *Notch1* morpholino oligonucleotides or miR-449 and *Dll1* morpholino oligonucleotides was also carried out, as indicated. Cilia are stained with an anti-acetylated-tubulin antibody (in red) and plasma membranes of injected cells are revealed by immunostaining against mGFP–CAAX. Note that *Dll1* mRNA injection suppressed ciliogenesis, although it increased the number of CCPs (Supplementary Fig. S8a). In contrast, both *Dll1* and *Notch1* knockdown enhanced ciliogenesis and rescued it in miR-449 morphants. (**c**) Quantification of the number of injected multiciliated cells (acetylated-tubulin positive cells) in each condition (several hundred cells were scored in each condition). $n = 777$, 535, 493, 916, 854, 690, 557 and 706 for control MO, miR-449 MOs, mir-449MOs + *DLL1* MO, *DLL1* MO, *DLL1* mRNA, P1P2 MO, *NOTCH1* MO, miR-449 MOs + *NOTCH1* MO, respectively. Error bars correspond to s.d.

specification. This may reflect widespread basal levels of expression of both *Dll1* and miR-449 that would be below the threshold of detection in physiological conditions, as predicted by the lateral inhibition model[30]. Alternatively, miR-449 knockdown and the associated rise in *Dll1* expression in CCPs may trigger increased *Dll1* expression in other cell types.

We found no evidence of a role for miR-449 in motile monociliated cells. Such cells are in charge of generating directional fluid flow and left/right asymmetry from midline structures of vertebrate embryos, including the gastrocoele roof plate in *Xenopus*[31]. No miR-449 expression could be detected in the gastrocoele roof plate and its knockdown did not impair left/right asymmetry (Supplementary Fig. S8b).

This and previous works indicate that activation of the Notch pathway represses multiciliogenesis in mammalian and frog mucociliary epithelia[27–29]. Here, we show that miR-449 expression is induced during multiciliogenesis and that miR-449-mediated inhibition of the Notch pathway is required for multiciliogenesis in our two models. miR-449 microRNAs target both DLL1 and NOTCH1 in HAECs, but only DLL1 in frog epidermis. We suggest that this difference is due to the different distribution of DLL1 in the two types of epithelium. DLL1 and NOTCH1 are present in proliferating HAECs, whereas they are both silenced in multiciliated HAECs through the action of miR-449. However, the levels of DLL1 and NOTCH1 expression remain high in surrounding cells (Fig. 4c–e). Consequently, CCPs are exposed to DLL1 from their neighbours and *Notch1* clearance by miR-449 is necessary to prevent Notch pathway activation and authorize multiciliogenesis. In *Xenopus* epidermis, CCPs are the main source of DLL1 (ref. 29). DLL1 clearance by miR-449 in CCPs is probably sufficient by itself to repress Notch signalling throughout the epidermis, thus bypassing the need for Notch1 targeting. Two other mechanisms could explain why *Dll1* downregulation in CCPs is necessary to stimulate multiciliogenesis in *Xenopus*. First, DLL1 may repress differentiation of CCPs through autocrine signalling. Second, DLL1 may activate Notch signalling in cells adjacent to CCPs, which in turn may produce a paracrine signal repressing CCP differentiation. Finally, we note that the expression of miR-449 remains elevated in differentiated cells, indicating that miR-449 microRNAs also play a role in maintaining the multiciliated phenotype.

Our work establishes the miR-449 family as an evolutionarily conserved key regulator of vertebrate multiciliogenesis. miR-449 microRNAs promote centriologenesis and contribute to terminal differentiation of multiciliated cells, by targeting both the cell cycle and the Delta/Notch pathway. Our study clearly illustrates that the development of multiciliated cells in the cellular environment of distinct tissues in distant animals involves common molecular networks. By providing new insights into the mechanisms controlling multiciliogenesis, our study may also pave the way for developing new therapeutic strategies aimed at treating pathologies associated with motile ciliary defects. □

METHODS

Methods and any associated references are available in the online version of the paper at http://www.nature.com/naturecellbiology

Note: Supplementary Information is available on the Nature Cell Biology website

ACKNOWLEDGEMENTS

This work was supported by CNRS, INSERM, Région Champagne-Ardenne, Région PACA, CG06 and by grants from ANR, Vaincre la Mucoviscidose, ARC and INCa. We thank V. Magnone, G. Rios, S. Fourré, K. LeBrigand and J. Maurizio, from the IBISA Functional Genomics Platform, S Antipolis, for help with transcriptome analyses and bioinformatics, F. Brau and J. Cazareth, for cellular imaging, V. Thomé for *in situ* hybridization experiments, F. Aguila for artwork and B. Mari for discussions. This work is the object of a CNRS patent N°09/03723.

AUTHOR CONTRIBUTIONS

B.M. led the project. P. Barbry, the Principal Investigator (IPMC), initiated and managed the entire project. L.K. is the Principal Investigator (IBDML) of the *Xenopus* section. B.M., L.K. and P. Barbry planned experiments, analysed and interpreted data and wrote the paper. B.M. and B. Chevalier carried out cell culture, cellular and molecular biology and cellular imaging in human, C.C., B.N-R. and T.J. carried out *in situ* hybridization experiments, cell culture and cell sorting on human tissues, G.L., M.C. and L.K. carried out *Xenopus* experiments, K.R-S. contributed to bioinformatics analyses, L-E.Z. and R.W. carried out HTS experiments, R.W. helped with manuscript correction, B. Cardinaud helped with molecular cloning, C.M. carried out Affymetrix transcriptome experiments and L.G-C. helped with PCR experiments. P. Birembaut provided critical discussion.

COMPETING FINANCIAL INTERESTS

The authors declare no competing financial interests.

Published online at http://www.nature.com/naturecellbiology
Reprints and permissions information is available online at http://www.nature.com/reprints

1. Fliegauf, M., Benzing, T. & Omran, H. When cilia go bad: cilia defects and ciliopathies. *Nat. Rev. Mol. Cell. Biol.* **8,** 880–893 (2007).
2. Shah, A. S. *et al.* Motile cilia of human airway epithelia are chemosensory. *Science* **325,** 1131–1134 (2009).
3. Wanner, A., Salathe, M. & O'Riordan, T. G. Mucociliary clearance in the airways. *Am. J. Respir. Crit. Care Med.* **154,** 1868–1902 (1996).
4. Hayes, J. M. *et al.* Identification of novel ciliogenesis factors using a new *in vivo* model for mucociliary epithelial development. *Dev. Biol.* **312,** 115–130 (2007).
5. Satir, P., Mitchell, D. R. & Jekely, G. How did the cilium evolve? *Curr. Top Dev. Biol.* **85,** 63–82 (2008).
6. Stubbs, J. L., Oishi, I., Izpisua Belmonte, J. C. & Kintner, C. The forkhead protein Foxj1 specifies node-like cilia in *Xenopus* and zebrafish embryos. *Nat. Genet.* **40,** 1454–1460 (2008).
7. Ambros, V. The functions of animal microRNAs. *Nature* **431,** 350–355 (2004).
8. Eulalio, A., Huntzinger, E. & Izaurralde, E. Getting to the root of miRNA-mediated gene silencing. *Cell* **132,** 9–14 (2008).
9. Ortholan, C. *et al.* MicroRNAs and lung cancer: new oncogenes and tumor suppressors, new prognostic factors and potential therapeutic targets. *Curr. Med. Chem.* **16,** 1047–1061 (2009).
10. LeSimple, P. *et al.* Trefoil factor family 3 peptide promotes human airway epithelial ciliated cell differentiation. *Am. J. Respir. Cell. Mol. Biol.* **36,** 296–303 (2007).
11. Marcet, B. *et al.* Extracellular nucleotides regulate CCL20 release from human primary airway epithelial cells, monocytes and monocyte-derived dendritic cells. *J. Cell. Physiol.* **211,** 716–727 (2007).
12. Coraux, C., Roux, J., Jolly, T. & Birembaut, P. Epithelial cell-extracellular matrix interactions and stem cells in airway epithelial regeneration. *Proc. Am. Thorac. Soc.* **5,** 689–694 (2008).
13. Lewis, B. P., Burge, C. B. & Bartel, D. P. Conserved seed pairing, often flanked by adenosines, indicates that thousands of human genes are microRNA targets. *Cell* **120,** 15–20 (2005).
14. Cardinaud, B. *et al.* miR-34b/miR-34c: a regulator of TCL1 expression in 11q-chronic lymphocytic leukaemia? *Leukemia* **23,** 2174–2177 (2009).
15. Flicek, P. *et al.* Ensembl 2008. *Nucleic Acids. Res.* **36,** D707 (2008).
16. Tamura, K., Dudley, J., Nei, M. & Kumar, S. MEGA4: molecular Evolutionary Genetics Analysis (MEGA) software version 4.0. *Mol. Biol. Evol.* **24,** 1596–1599 (2007).
17. Dawe, H. R., Farr, H. & Gull, K. Centriole/basal body morphogenesis and migration during ciliogenesis in animal cells. *J. Cell. Sci.* **120,** 7–15 (2007).
18. Pearson, C. G., Culver, B. P. & Winey, M. Centrioles want to move out and make cilia. *Dev. Cell.* **13,** 319–321 (2007).
19. Vladar, E. K. & Stearns, T. Molecular characterization of centriole assembly in ciliated epithelial cells. *J. Cell. Biol.* **178,** 31–42 (2007).
20. Hajj, R. *et al.* Basal cells of the human adult airway surface epithelium retain transit-amplifying cell properties. *Stem. Cells.* **25,** 139–148 (2007).
21. Le Brigand, K., Robbe-Sermesant, K., Mari, B. & Barbry, P. MiRonTop: mining microRNAs targets across large scale gene expression studies. *Bioinformatics* **26,** 3131–3132 (2010).
22. Zhen, G. *et al.* IL-13 and epidermal growth factor receptor have critical but distinct roles in epithelial cell mucin production. *Am. J. Respir. Cell. Mol. Biol.* **36,** 244–53 (2007).
23. Feng, M. & Yu, Q. miR-449 regulates CDK-Rb-E2F1 through an auto-regulatory feedback circuit. *Cell Cycle* **9,** 213–214 (2010).
24. Lize, M., Pilarski, S. & Dobbelstein, M. E2F1-inducible microRNA 449a/b suppresses cell proliferation and promotes apoptosis. *Cell. Death. Differ.* **17,** 452–458 (2009).
25. Yang, X. *et al.* miR-449a and miR-449b are direct transcriptional targets of E2F1 and negatively regulate pRb-E2F1 activity through a feedback loop by targeting CDK6 and CDC25A. *Genes Dev.* **23,** 2388–2393 (2009).
26. Choi, W. Y., Giraldez, A. J. & Schier, A. F. Target protectors reveal dampening and balancing of Nodal agonist and antagonist by miR-430. *Science* **318,** 271–274 (2007).
27. Tsao, P. N. *et al.* Notch signalling controls the balance of ciliated and secretory cell fates in developing airways. *Development* **136,** 2297–2307 (2009).
28. Guseh, J. S. *et al.* Notch signalling promotes airway mucous metaplasia and inhibits alveolar development. *Development* **136,** 1751–1759 (2009).
29. Deblandre, G. A., Wettstein, D. A., Koyano-Nakagawa, N. & Kintner, C. A two-step mechanism generates the spacing pattern of the ciliated cells in the skin of *Xenopus* embryos. *Development* **126,** 4715–4728 (1999).
30. Marnellos, G., Deblandre, G. A., Mjolsness, E. & Kintner, C. Delta-Notch lateral inhibitory patterning in the emergence of ciliated cells in *Xenopus*: experimental observations and a gene network model. *Pac. Symp. Biocomput.* 329–340 (2000).
31. Essner, J. J *et al.* Conserved function for embryonic nodal cilia. *Nature* **418,** 37–38 (2002).

DOI: 10.1038/ncb2241

METHODS

Subjects/tissue samples. Inferior turbinates or nasal polyps were from patients who underwent surgical intervention for nasal obstruction or septoplasty (provided by L. Castillo, Pasteur Hospital, Nice, France; T. Nasser, Courlancy Clinic, Reims, France; and C. Ruaux, La Sagesse Hospital, Rennes, France). The use of human tissues was authorized by the bioethical law 94-654 of the French Public Health Code and written consent from the patients.

Isolation, culture and sorting of HAECs. Primary HAECs were cultured according to refs 10,11. Experiments were conducted on cultures with transepithelial electrical resistance above 500 $\Omega\,cm^{-2}$. DAPT (*N*-[*N*-(3,5-difluorophenacetyl)-L-alanyl]-*S*-phenylglycine *t*-butyl ester) was used (10 μM, incubated from ALI-D0 until terminal differentiation) to inhibit the Notch pathway, when indicated. For cell sorting (three donors), we used the human-specific basal cell markers tetraspanin CD151 and tissue factor to separate basal cells from columnar cells with a FACSAria cell sorter (BD Biosciences), as described previously[20].

***Xenopus* injections.** Eggs obtained from NASCO females were fertilized *in vitro*, dejellied, cultured and injected as described[32]. Capped *Dll1* (ref. 29) and *centrin-2–mGFP* (ref. 33) cRNAs were generated with the Ambion mMessage Machine kit. pCS105–mGFP–CAAX (a gift from C. Chang, University of Alabama at Birmingham, USA) was linearized with AseI and cRNA was synthesized with Sp6 polymerase. Fixable fluorescent lysine dextran (FLDx, 2.5 ng per cell) was co-injected with morpholino oligonucleotides to sort injected embryos, and anti-fluorescein immunodetection was carried out to trace the distribution of morpholino oligonucleotides in fixed embryos. All injections were done at least twice.

Immunohistochemistry. Frozen sections or fresh cultures of ALI-D21 HAECs or bronchial tissue sections were used for detection of β4-tubulin, cytokeratin-13, Muc5AC, CDC20B and nuclei as described previously[10,20]. We also used anti-centrin-2 mouse monoclonal antibody (clone (*N*-17)-R; 1:200, Santa Cruz Biotechnology), anti-CDC20B mouse monoclonal antibody (clone 2F2; 1:400, Sigma) and rabbit polyclonal antibodies to DLL1 or mouse monoclonal anti-NOTCH1 (clone A6; 1:200, Abcam). *Xenopus* multiciliated cells were stained with anti-acetylated tubulin monoclonal antibody (clone 6-11B-1, 1:200, Sigma). To reveal the mGFP–CAAX, we used a rabbit anti-mGFP antibody (1:400; Torrey Pines Biolabs) together with a secondary antibody coupled to Alexa 488 (Molecular Probes). Secondary antibodies were used at 1:200 or 1:500 according to the experiments.

Western blot and ELISA measurement. Preparation of HAEC protein lysate (3 donors) was carried out using RIPA buffer (Thermo Scientific Pierce) and western blotting using NuPage Novex Bis Tris MiniGels (Invitrogen) following the manufacturer's instructions. Revelation was carried out with immobilon ECL (Millipore); gel images were acquired using a Fujifilm LAS-3000 imager. In addition to the antibodies mentioned above, we used anti-CCNE2 (1:200, a gift from G. Ponzio, INSERM U 634, UFR Médecine, Nice, France), rabbit polyclonal anti-NOTCH1 (1:500, Abcam) and anti-β-actin antibodies (1:1,000, I-19, Santa Cruz Biotechnology).

Apical and basolateral supernatants of untreated, miR-Neg- or miR-449a-treated HAECs (two donors) were taken after 48 h of treatment. Released amphiregulin (AREG) was then measured using a DuoSet ELISA kit (R&D systems) following the manufacturer's instructions.

Total RNA extraction. HAECs (a total of 16 donors) were lysed in TRIZOL reagent (Invitrogen). *Xenopus* ectoderm explants were prepared at late blastula stage, cultured in 1×MBS (88 mM NaCl, 1 mM KCl, 0.7 mM $CaCl_2$, 1 mM $MgSO_4$, 5mM HEPES at pH 7.8 and 2.5 mM $NaHCO_3$) and collected for RNA extraction at gastrula stage 11.5 and tailbud stage 26. *Xenopus* total RNAs were purified with a Qiagen RNeasy kit (Qiagen). The integrity of RNA was evaluated using RNA nano-chips (Agilent Technologies).

microRNA HTS and microarray experiments. Total RNAs were isolated from ALI cultures (three donors) or sorted HAECs (three donors) and from stage 11.5 (gastrula) and stage 26 (tailbud) epidermal explants of *Xenopus* embryos (pool of $n = 50$ explants of each stage). Small RNA libraries were generated from total RNA (300 ng) with the SOLiD Small RNA Expression Kit (SREK, Applied Biosystems) and sequenced on the Applied Biosystems SOLiD System following the manufacturer's instructions. Reads ($5–20 \times 10^6$ per sample) were matched to both known microRNA precursors and to the human or *Xenopus tropicalis* genome using the Applied Biosystems RNA2map software. All table results were submitted to GEO (GSE22147). Parameters for the *Xenopus* analysis took into account the fact that the list of microRNA precursors was from *Xenopus tropicalis* rather than from *Xenopus laevis*.

MicroRNA profiling was carried out using microarrays (Human microRNA Microarray v2, containing 866 human and 89 human viral microRNAs, Sanger microRNABase v.12.0, Agilent Technologies), according to the supplier prescription.

mRNA expression profiling was carried out with DNA GeneChip Human Gene 1.0 ST Array (Affymetrix), according to the manufacturer's instructions. Data were processed using RMA (Robust Multi-Chip Average)[34].

All data were stored on microarray information system Mediante[35], and analysed with Bioconductor (http://www.bioconductor.org). Results have been submitted to GEO (accession number GSE22147) (http://www.ncbi.nlm.nih.gov/geo/query/acc.cgi?acc=GSE22147).

Quantitative RT–PCR. Real-time PCR was carried out using a TaqMan MicroRNA Assay (Applied Biosystems) on a Lightcycler 480 (Roche), according to the manufacturer's instructions. The expression levels of mature microRNAs were calculated using the 2-deltaCT method, using RNU44 and RNU6B as endogenous controls.

***In situ* hybridization.** After fixation in 4% paraformaldehyde (Electron Microscopy Sciences), frozen sections of ALI-D21 cultures or of human airway tissues were acetylated, and incubated overnight at 55 °C with 0.3 $ng\,\mu l^{-1}$ locked nucleic acid (LNA) digoxigenin-labelled microRNA probes (Exiquon) in 50% deionized formamide, 0.3 M NaCl, 20 mM Tris-HCl at pH 8.0, 5 mM EDTA, 10 mM $NaPO_4$ at pH 8.0, 10% dextran sulphate, 1× Denhardt's solution and 0.5 $mg\,ml^{-1}$ yeast RNA. The probes were: miR-449, 5′-ccagctaacaatacactgcc-3′; miR-31, 5′-agctatgccagcatcttgcct-3′; scramble microRNAs, 5′-gtgtaacacgtctatacgccca 3′. Probes were revealed by sequential incubations with horseradish-peroxidase-conjugated sheep anti-digoxigenin antibodies (Roche), the Tyramide Signal Amplification Plus DNP AP System (Perkin-Elmer) and BCIP/NBT substrate (DakoCytomation). Some slides were then exposed to mouse anti-Muc5AC antibodies and revealed with the LSAB2 System-HRP kit (Dako). Sections were counterstained with Nuclear Fast Red eosin/safran, and mounted using Eukitt mounting medium (Electron Microscopy Sciences).

Isolated HAECs from three donors (5×10^4 cells per slide in 100 μl PBS) were centrifuged (55*g*, 10 min) using cytospin 2 (Shandon). Slides were air-dried (1 h), fixed in cold-methanol plus acetone (10 min), air-dried again and stored at −80 °C. *In situ* hybridization and immunocytochemistry were then carried out as before to visualize and quantify cells co-expressing miR-449 and β4-tubulin.

In *Xenopus*, we used an anti-miR-449a mono-digoxigenin-labelled LNA probe (Exiqon). *In situ* hybridization was done as described previously[33]. Antisense riboprobes for α-tubulin[29], *Dll1* (ref. 29), *Tex15* (ref. 36) and *Foxj1* (ref. 37) were prepared as described in the respective references.

miR-449 and target gene knockdown experiments. *HAECs.* 3′-cholesterol-linked 2′-*O*-methyl miR-449a/b antisense oligonucleotide (antagomiR), 5′-$a_s c_s c_s$agcuaacaauacacugc$_s c_s$a-Chol-3′ and Notch1 protector oligonucleotide 5′-$a_s a_s a_s$aaggcaguguuucugu$_g u_s$a-Chol-3′ (phosphorothioate bonds are indicated by subscript s) were purchased from Eurogentec. miR-449 antagomiR targets *Homo sapiens* miR-449a (full match) and miR-449b with one mismatch. The Notch1 protector is a complementary antisense oligonucleotide targeting the conserved miR-449-binding site of the human *Notch1* 3′-UTR. The negative control was the Clear-miR (5′-$c_s a_s u_s$cgucgaucguagcg$_s c_s$a-Chol-3′) from Eurogentec. AntagomiR or antisense protector (100 μM) was pre-incubated with fetal calf serum (FCS) for 30 min at room temperature. Then, the antagomiR/FCS or Notch1 protector/FCS mixture in differentiation medium (20 μM) was added to the apical side of primary HAECs. After 2 h at 37 °C, the apical medium was removed to restore the air–liquid interface. Transfection was repeated every 5 days with freshly prepared antagomiR or antisense protector, until control cells reached full differentiation (typically after 21 days).

Xenopus embryos. Morpholino oligonucleotides against miR-449 (GeneTools, LLC) were antisense to *Xenopus tropicalis* miR-449: miR-449a morpholino oligonucleotide, 5′-ACCAGCTAACATTACACTGCCT-3′; miR-449b morpholino oligonucleotide, 5′-GCCAGCTAAAACTACACTGCCT-3′; miR-449c morpholino oligonucleotide, 5′-ACAGCCAGCTAGCAAGTGCACTGCC-3′; morpholino oligonucleotide control, 5′-TGCACGTTTCAATACAGACCGT-3′. We used previously reported morpholino oligonucleotides against *Dll1* (ref. 38) and *Notch1* (ref. 39). The protector morpholino oligonucleotides directed against miR-449-binding sites in *Dll1* 3′-UTR have the following sequences: P1 morpholino oligonucleotide, 5′-CGGCAGTGCAACAGTTTATGTCTGG-3′; P2 morpholino oligonucleotide, 5′-AGGCAGTGACTGTCTGTAGTTTAGC-3′.

Ectopic expression of microRNAs in HAECs. HAECs (four donors) were grown to 30% confluency in proliferation medium. Cells were then transfected with microRNAs (10 nM) using Lipofectamine RNAi Max Reagent (Invitrogen) in OPTIMEM (Invitrogen), and RNA was extracted 48 h later.

Cell cycle analysis by flow cytometry. A549 lung adenocarcinoma cells, grown in DMEM supplemented with L-glutamine and 10% FCS at 30% confluency, were first synchronized by overnight serum starvation and transfected with microRNAs. Cells were collected 48 h later, fixed with 80% ethanol and stained (37 °C, 30 min) with 0.1 ml propidium iodide solution (50 μg ml^{-1}) containing RNAse A (50 μg ml^{-1}). Data were acquired on a FACScalibur flow cytometer (Becton-Dickinson). Percentages of cells in G1, S and G2+M were calculated using CellQuest Pro software.

Viability and apoptosis measurements. HAECs (two donors in triplicate) were chronically treated with antagomiR (20 μM) as before and viability was measured 24 h, 14 days and 21 days later using a resazurin-based *in vitro* toxicology assay kit (Sigma), following the manufacturer's instructions.

In *Xenopus*, apoptosis was evaluated through terminal deoxynucleotidyl transferase-mediated dUTP nick end labelling. Briefly, fixed embryos were incubated with TdT enzyme (Invitrogen) and digoxigenin-labelled ddUTP nucleotides (Roche) to label DNA fragments in apoptotic cells. Digoxigenin-labelled molecules were then immunodetected with an anti-digoxigenin antibody coupled to alkaline phosphatase and staining was done with NBT/BCIP substrate.

Plasmid constructs and luciferase measurements. Complete or partial sequences from the wild-type or mutant 3′-UTRs of *Areg*, *Ccnb1*, *Ccne2*, *Cdc25a*, *Dll1* and *Notch1* were amplified and cloned into psiCheck2 vector (Promega). For mutated 3′-UTRs, three bases of each seed region were changed by complementary bases. psiCheck2 constructions were co-transfected with synthetic microRNAs or a negative control (Ambion, Applied Biosystems) with or without antagomiRs or antisense protectors into HEK293T cells, and luciferase activities were measured as previously described[40].

32. Marchal, L., Luxardi, G., Thome, V. & Kodjabachian, L. BMP inhibition initiates neural induction via FGF signalling and Zic genes. *Proc. Natl Acad. Sci. USA* **106,** 17437–17442 (2009).
33. Mitchell, B. *et al.* A positive feedback mechanism governs the polarity and motion of motile cilia. *Nature* **447,** 97–101 (2007).
34. Irizarry, R. A. *et al.* Exploration, normalization, and summaries of high density oligonucleotide array probe level data. *Biostatistics* **4,** 249–264 (2003).
35. Le Brigand, K. & Barbry, P. Mediante: a web-based microarray data manager. *Bioinformatics* **23,** 1304–1306 (2007).
36. Kloosterman, W. P. *et al.* *In situ* detection of miRNAs in animal embryos using LNA-modified oligonucleotide probes. *Nat. Methods* **3,** 27–29 (2006).
37. Pohl, B. S. & Knochel, W. Isolation and developmental expression of *Xenopus* FoxJ1 and FoxK1. *Dev. Genes. Evol.* **214,** 200–205 (2004).
38. Morichika, K. *et al.* Perturbation of Notch/Suppressor of Hairless pathway disturbs migration of primordial germ cells in *Xenopus* embryo. *Dev. Growth. Differ.* **52,** 235–244 (2010).
39. Lopez, S. L. *et al.* Notch activates sonic hedgehog and both are involved in the specification of dorsal midline cell-fates in *Xenopus*. *Development* **130,** 2225–2238 (2003).
40. Pottier, N. *et al.* Identification of keratinocyte growth factor as a target of microRNA-155 in lung fibroblasts: implication in epithelial-mesenchymal interactions. *PLoS One* **4,** e6718 (2009).

nature cell biology

DOI: 10.1038/ncb2241

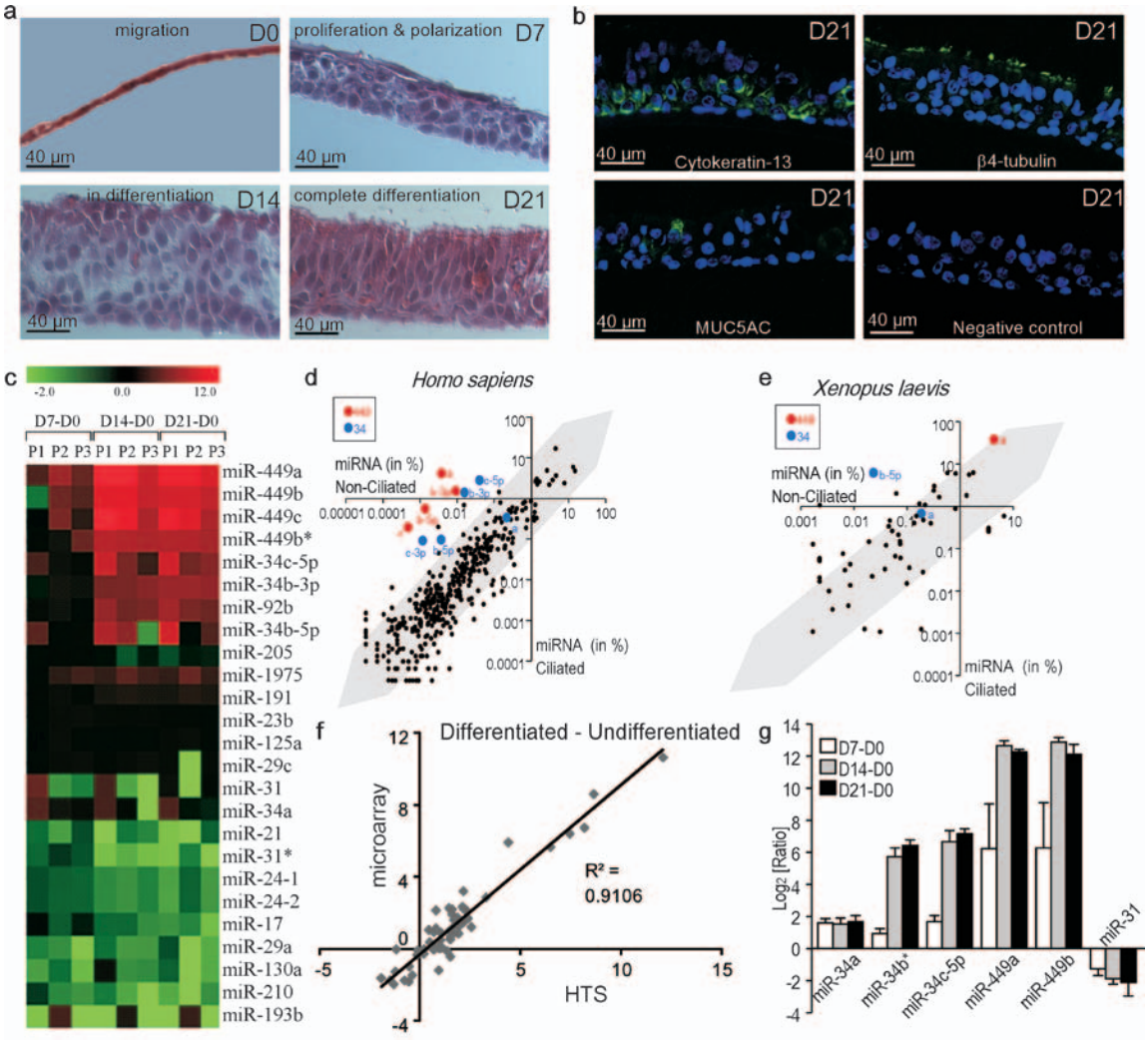

Figure S1 microRNA signature during multiciliogenesis in HAECs and *Xenopus laevis* embryonic epidermis. (a) Characterization of *in vitro* regeneration of human airway mucociliary epithelium, mainly constituted of columnar multiciliated and mucus-secretory cells and basal cells. In native upper airways, multiciliated cells typically represent ~50% of HAECs[11], mucus-secretory cells account for ~20% of HAECs[37], and basal cells represent ~30% of HAECs[17]. In contrast, mucus-secretory cells account for less than 1% of HAECs in primary cultures. Four typical steps of the culture are illustrated: (1) ALI-D0, monolayer of undifferentiated cells undergoing migration and proliferation; (ii) ALI-D7, transient squamous and pluristratified epithelium , starting polarization; (iii) ALI-D14, initiation of mucociliary differentiation; iv) ALI-D21, pseudostratified well-differentiated mucociliary epithelium. (b) immunohistochemical characterization of well differentiated cultures (ALI-D21), containing multiciliated cells, mucus-secretory cells and basal cells, detected with antibodies against β4-tubulin, Muc5AC, and cytokeratin-13 antibodies, respectively. Nuclear labelling with DAPI (blue). (c) Heat map showing the fold-changes of microRNAs expression in HAECs at D7, D14 and D21 of air liquid interface relative to D0 (3 patients, P1-P3). miR-21 decreased from 14.7±1.7% in proliferating cells to 5.0±4.0% at the onset of multiciliogenesis. miR-191 increased from 4.35±0.85% in proliferating cells to 17.7±1%, in well-differentiated airway epithelium. miR-34a was up-regulated during polarization but never represented more than 1% of all detected sequences. The most dramatic changes occurred for 23 microRNAs at the onset of multiciliogenesis (ALI-D14): miR-449a, miR-449b, miR-449b*, miR-449c, miR-34a, miR-34b-3p, miR-34b-5p, miR-34c-5p, miR-92b, miR-191, miR-1975, miR-125a were dramatically increased, while miR-17, miR-193b, miR-31, miR-31*, miR-130a, miR-205, miR-21, miR-24-1, miR-24-2, miR-210, miR-29a were decreased. miR-449abc, miR-34bc, and miR-92b barely detected in proliferating cells, were robustly upregulated after differentiation. MicroRNA expression appeared stable at later time points. (d, e) Scatter plots of the relative microRNAs abundance (% of total microRNAs reads) in undifferentiated (non-ciliated) (ALI-D0, x-axis) *versus* differentiated (multiciliated) (ALI-D21, y-axis) HAEC cultures (d) and in *Xenopus* epidermal explants from embryos before (E11.5, x-axis) and after (E26, y-axis) the onset of multiciliogenesis (e). The miR-449 and miR-34 families are indicated in red and blue, respectively. Zones with <10-fold variation are shaded in grey. (f) Correlation between HTS (SOLiD, Applied Biosystems) and microarray (Agilent Technologies) data in HAECs. Log2(ratios) between differentiated and undifferentiated cells (n=3 donors) between HTS and microarray experiments were compared (coefficient of correlation $R^2 = 0.91$). (g) Real time PCR validation of miR-449, miR-34 and miR-31 in HAECs. Data are means ± s.d. from five individual experiments

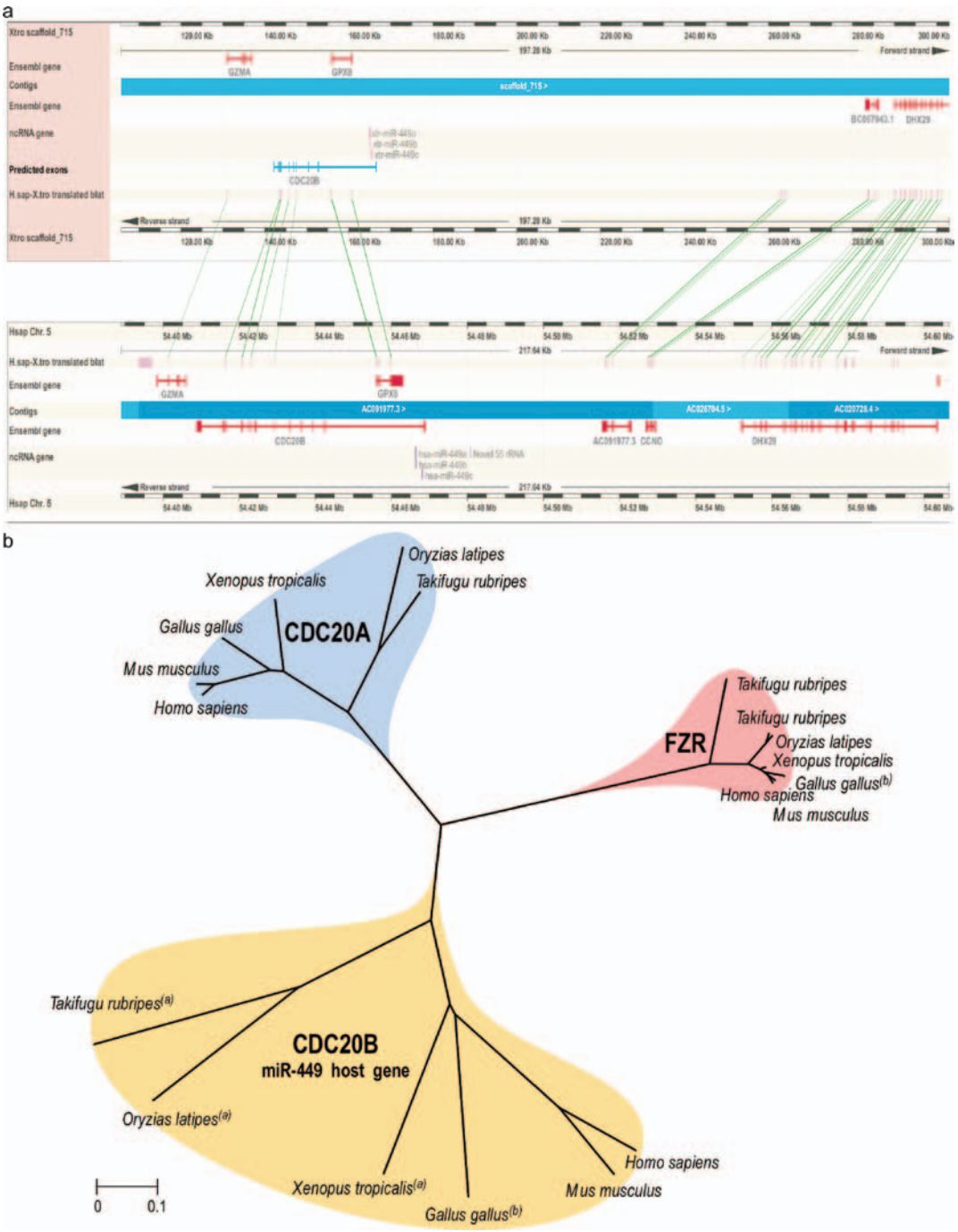

Figure S2. (a) Synteny of the miR-449 genomic region. Ensembl multi-species view of human and *Xenopus tropicalis* miR-449 genomic region[38]. Custom data for *Xenopus tropicalis* (and not *Xenopus laevis*, which is not yet available) predicted miR-449 and predicted *Cdc20b* exons were uploaded in gff format. The representation of this region shows that gene order is conserved between human and amphibian. *Cdc20b* is located upstream to *Gzma* and downstream to *Ccno*, *Dhx29*, and an uncharacterized gene similar to *Geminin*. *MiR-449* cluster genomic location is conserved, in the second intron of *Cdc20b,* next to *Gpx8* gene located on the opposite strand. **(b)** Unrooted phylogenetic tree of the CDC20 family in vertebrates. Known protein sequences of CDC20A, CDC20B and FZR (Fizzy related) were retrieved from Ensembl release 56. Protein sequences of CDC20B for *X. tropicalis*, *A. carolinensis, T. rubripes, O. latipes, G. gallus* were established by a combination of tblastx analysis of each syntenic region as well as blastx analysis using the available *Cdc20b* sequences as database and Genscan analysis on the genomic sequence (after exclusion of the *Gpx8* gene region). Multiple alignments were completed using ClustalW and the unrooted tree was constructed using the Neighbor-Joining method with pairwise deletion option in MEGA 4[39]. The evolutionary distances were computed using the Poisson correction method and are in the units of the number of amino acid substitutions per site. All positions containing alignment gaps and missing data were eliminated in pairwise sequence comparisons. All analyzed vertebrates contain at least one member of each family, *Cdc20a*, *Cdc20b* and *Fzr*. Each *Cdc20b* gene hosts a miR-449 cluster. *(a) predicted sequence (b) corrected sequence.*

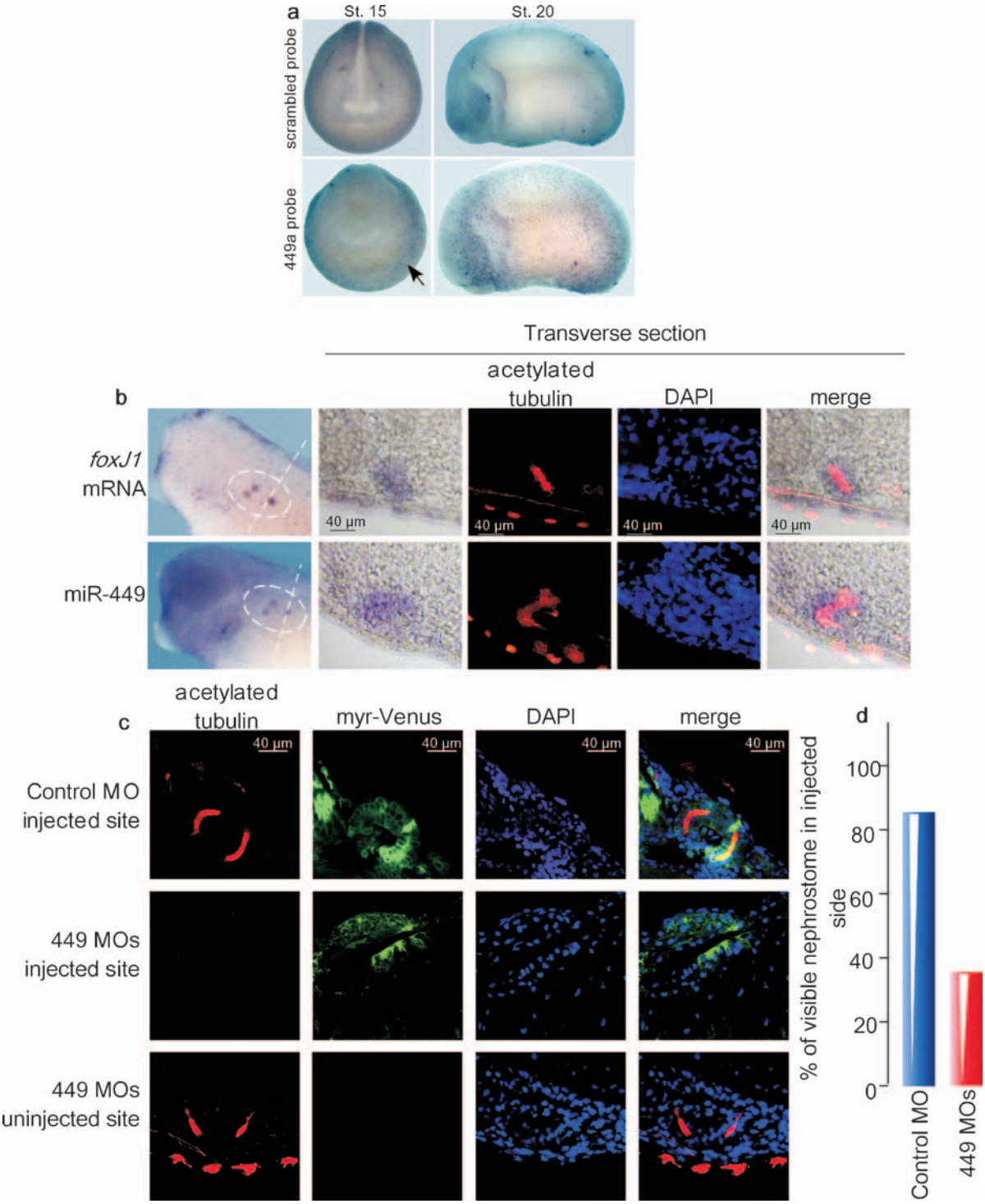

Figure S3 (a) *Xenopus* miR-449 are expressed at an early stage of differentiation. Whole-mount *ISH* was performed at open neural plate stage (st. 15) and early tailbud stage (st. 20), with a digoxigenin-labeled LNA probe against miR-449a or a scramble LNA probe, as negative control. Note that punctate staining (see Fig. 1) is visible with the anti-miR-449a/b probe at stage 15 (arrow), which is before acetylated-tubulin staining can be detected. **(b-d)** miR-449 is expressed in multiciliated cells of the nephrostomes and required for their ciliogenesis. (b) Comparison of *foxJ1* mRNA and miR-449 distribution in the three nephrostomes (encircled in white) of the pronephros at tailbud stage 35. Embryos were transversally sectioned and double stained with antibodies against acetylated-tubulin to reveal cilia. Note the co-localization of *foxJ1* and miR-449 with cilia of nephrostomic cells. (c) 8-cell embryos were unilaterally injected in the marginal zone to target the pronephros territory with control or miR-449 MOs, together with myr-Venus mRNA as a lineage tracer. Stage 35 embryos were transversally sectioned and stained for cilia. (d) Quantification of the reduction in the number of ciliated nephrostomes detectable in miR-449 morphants. Quantification was done on the injected half.

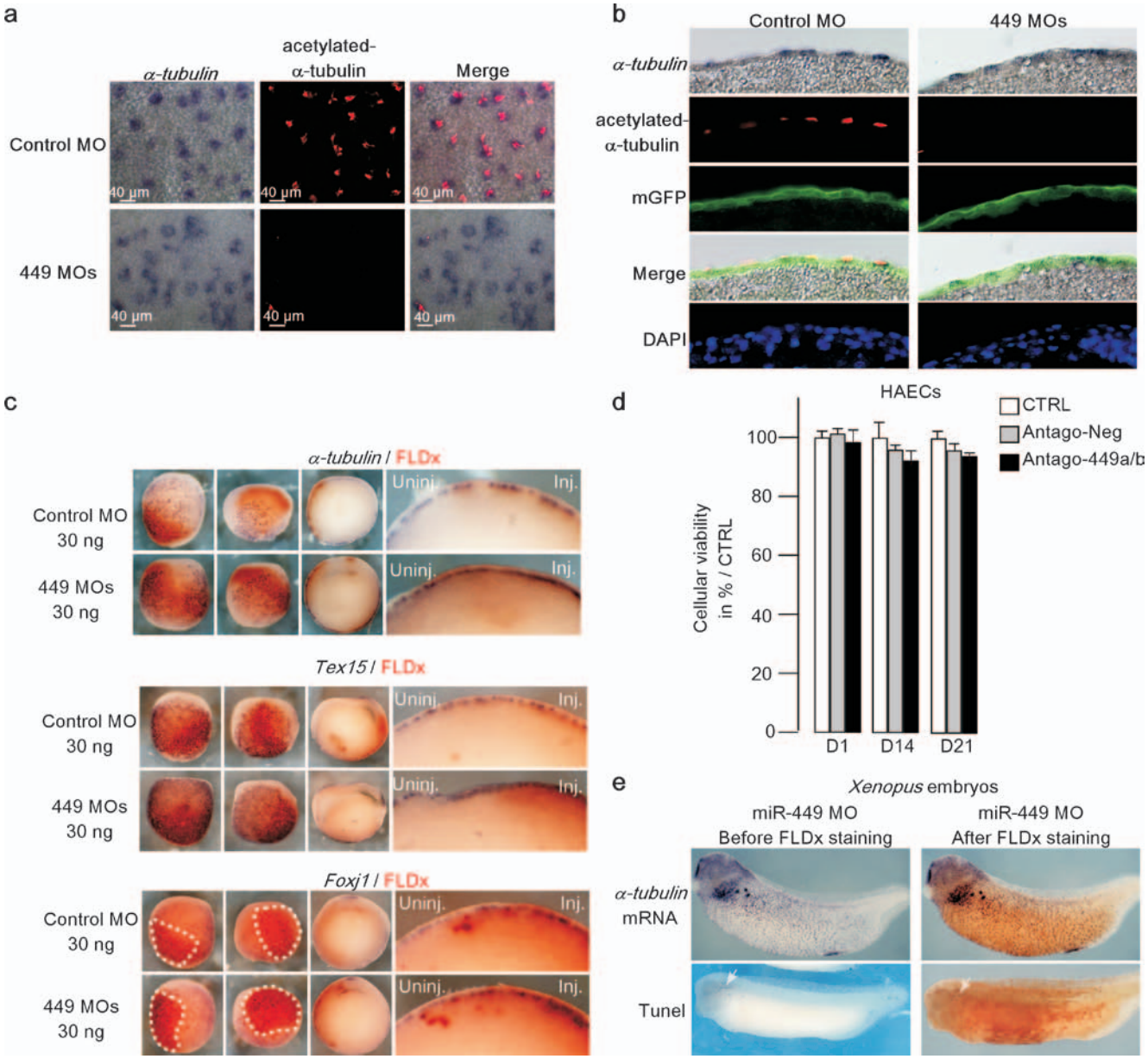

Figure S4 (a-b) miR-449 deficient cells intercalate in the superficial epidermal layer, maintain a ciliated cell progenitor identity but do not make cilia. 16-cell embryos were injected in the epidermis with miR-449 MOs or control MO, together with GFP-CAAX as a lineage tracer. Embryos were fixed at tailbud stage 25 and processed for *α-tubulin ISH* and acetylated-tubulin immunostaining. (a) Whole embryos were photographed, showing that CCPs are maintained in miR-449 deficient embryos but do not build cilia. (b) Embryos were transversally sectioned to examine the position of the *α-tubulin* positive cells in the epidermis. This shows that miR-449-deficient CCPs are capable of intercalating in the outer epithelial layer but do not build cilia. **(c)** miR-449 knock-down enhances ciliated cell specification. Cleavage stage embryos were injected in the epidermis with a mixture of anti-miR-449 MOs or control MO and FLDx, as indicated. Embryos fixed at early neurula stage were subjected to *ISH* with *α-tubulin*, *Tex15* and *Foxj1* riboprobes, followed by immunostaining to reveal the presence of FLDx in brown. Embryos were then sectioned to better visualize the density of ciliated cell progenitors in injected domains. For all three markers, the miR-449 knockdown increased the number of CCPs. **(d-e)** miR-449 knockdown does not alter cell viability and does not cause apoptosis. (d) HAECs viability was measured using resazurin-based in vitro toxicology assay kit after one day (D1), 14 days (D14) or 21 days (D21) of treatment with Antago-449a/b compared to Antago-Neg and untreated cells (CTRL). Data are means ± s.d. from six individual experiments. Treatments with antago-449a/b failed to alter cellular viability of differentiating HAECs. (e) 16-cell embryos were injected in the epidermis with miR-449 MOs and FLDx, as a lineage tracer. Embryos were fixed at tadpole stage 35 and processed for *α-tubulin ISH* and TUNEL staining. Embryos were photographed before and after FLDx staining in brown. miR-449 deficient cells maintain a ciliated cell progenitor identity and do not display significant tunel staining (n=25). The previously described TUNEL staining in the head region at this stage (white arrow) served as control for the procedure.

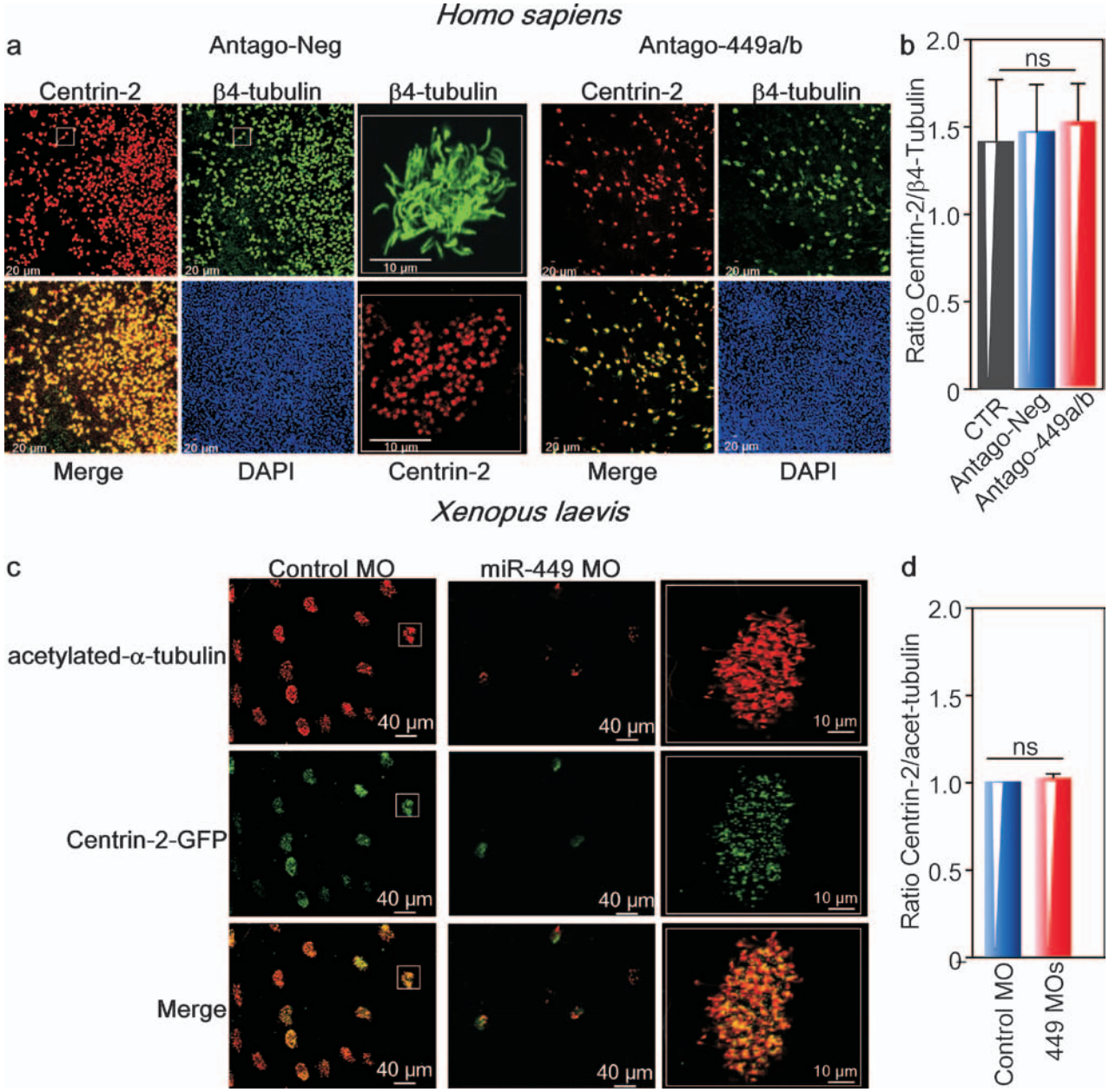

Figure S5 miR-449 knockdown suppresses centriologenesis and multiciliogenesis. (a) HAECs cultures were treated with antagomiR-449 (antago-449a/b), used to block both miR-449a and b, which were the most abundant miR-449, or negative control antagomiR (antago-Neg) during regeneration, as indicated. Cultures were fixed at ALI-D21 (terminal differentiation stage) and co-immunostained with anti-β4-tubulin and anti-centrin-2 antibodies. β4-tubulin-positive or centrin-2 positive multiciliated cells were visualized and quantified by confocal videomicroscopy with 10X objective. Multiple cilia and hundreds of basal bodies per cell were visualized using 63X objective. Note that miR-449 knock-down inhibited cilia formation and basal body multiplication in the same cells. On the contrary, control antagomiR (Antago-Neg) failed to affect centriologenesis (centrin-2 positive cells) as well as multiciliogenesis (β4-tubulin positive cells). (b) The ratio between centrin-2 positive cells and β4-tubulin positive cells was similar among conditions, indicating that miR-449 invalidation altered both centriologenesis and multiciliogenesis. (c) 16-cell embryos were injected in the epidermis with a mixture of anti miR-449 MOs or control MO and 400 pg/cell *centrin2-GFP* mRNA, to stain basal bodies. Embryos were fixed at tailbud stage and processed for acetylated-tubulin immunostaining. Note the concomitant loss of cilia and basal body staining in miR-449 deficient embryos. (d) Similarly to HAECs, *Xenopus* miR-449 knockdown caused a parallel reduction in the number of cells positive for both tubulin and centrin-2, suggesting that miR-449 blocked multiciliogenesis at an early step by acting before centriologenesis. In control cells, multiple cilia and basal bodies were visualized using 20x objective.

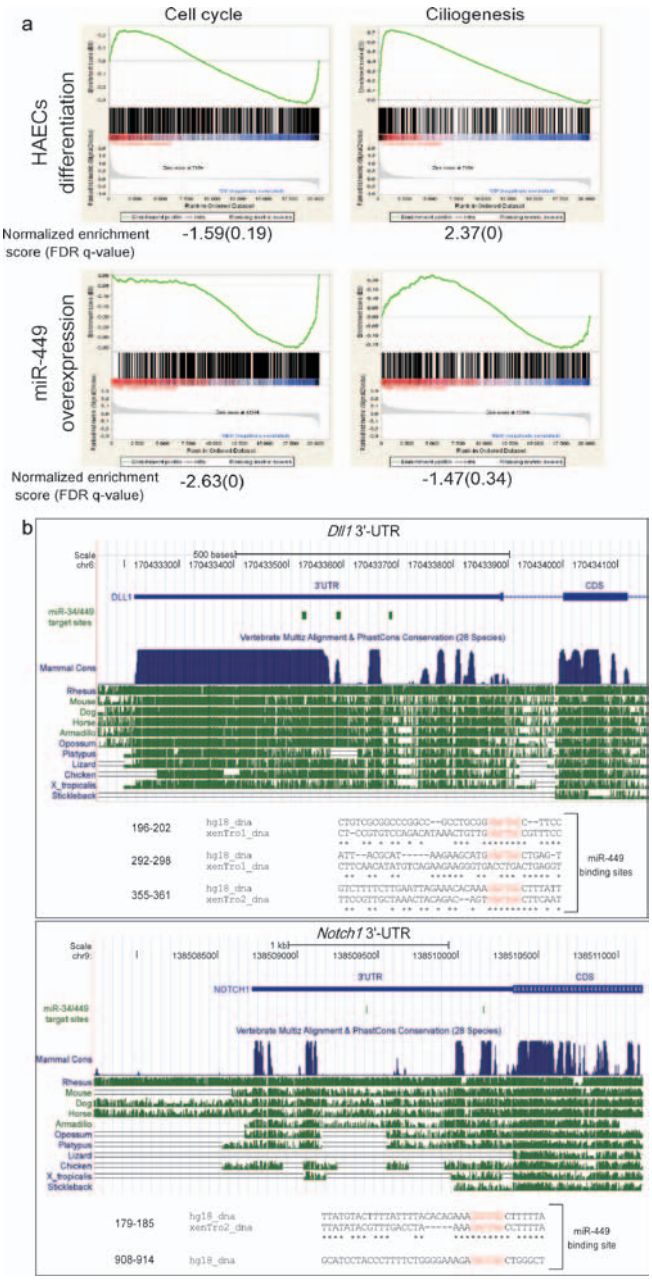

Figure S6 (a) Identification of putative miR-449 targets in HAECs. In order to define ciliogenesis-associatedmiR-449 targets, we characterized the transcriptional program during differentiation and after the transfection of each individual miR-449 into proliferating HAECs. Functional annotation of these experiments with Gene Set Enrichment Analysis (GSEA) revealed a significant enrichment in genes related to "cell cycle" (particularly the G2/M checkpoint), and to "ciliogenesis" (including Notch signalling players). In the miR-449 overexpression condition, "cell cycle", but not "ciliogenesis", was significantly enriched. The 4 pictures summarize the results of a gene set enrichment analysis, as explained at http://www.broadinstitute.org/gsea/doc/GSEAUserGuideFrame.html. GSEA calculates an enrichment score (ES), which reflects the degree to which a gene set is overrepresented at the top or bottom of a ranked list of genes. A positive ES indicates gene set enrichment at the left of the ranked list (corresponding to an up-regulation of the gene set); a negative ES indicates gene set enrichment at the right of the ranked list (corresponding to a down-regulation of the gene set). For each panel, the top plot provides a graphical view of the enrichment score for the gene set indicated on the left. The middle portion of the plot shows where the members of the gene sets ("cell cycle" or "ciliogenesis") appear in the ranked list of genes. The bottom portion of the plot shows the value of the ranking metric, which measures a gene's correlation with a phenotype. A positive value indicates correlation with the first phenotype (differentiation or miR-449 over-expression) and a negative value indicates correlation with the second phenotype (non-differentiated or control). miR-449 transfection of cells grown on plastic, which cannot fully differentiate into ciliated cells, probably explains the absence of a significant enrichment for the "ciliogenesis" term. All experimental data have been stored on Gene Expression Omnibus under the accession numbers GSE22147. **(b)** Conservation,of miR-449 binding sites on *Dll1*- and *Notch1*- *3'*-UTRs. Genomic region surrounding 3'UTR of *Dll1* and *Notch1* gene are displayed using the UCSC Genome Browser on Human March 2006 (NCBI36/hg18) Assembly (http://genome.ucsc.edu/). The miR-449/miR-34 target site positions in the 3' UTR of the human *Dll1* gene and *Notch1* are represented. Multiple phastCons alignments of mammalian species and pairwise alignments of each species to the human genome show conserved genomic regions. For each target site position in the 3'UTR, the human genomic region sequence is displayed. When conserved, *Xenopus tropicalis* genomic region is aligned to the human target site region.

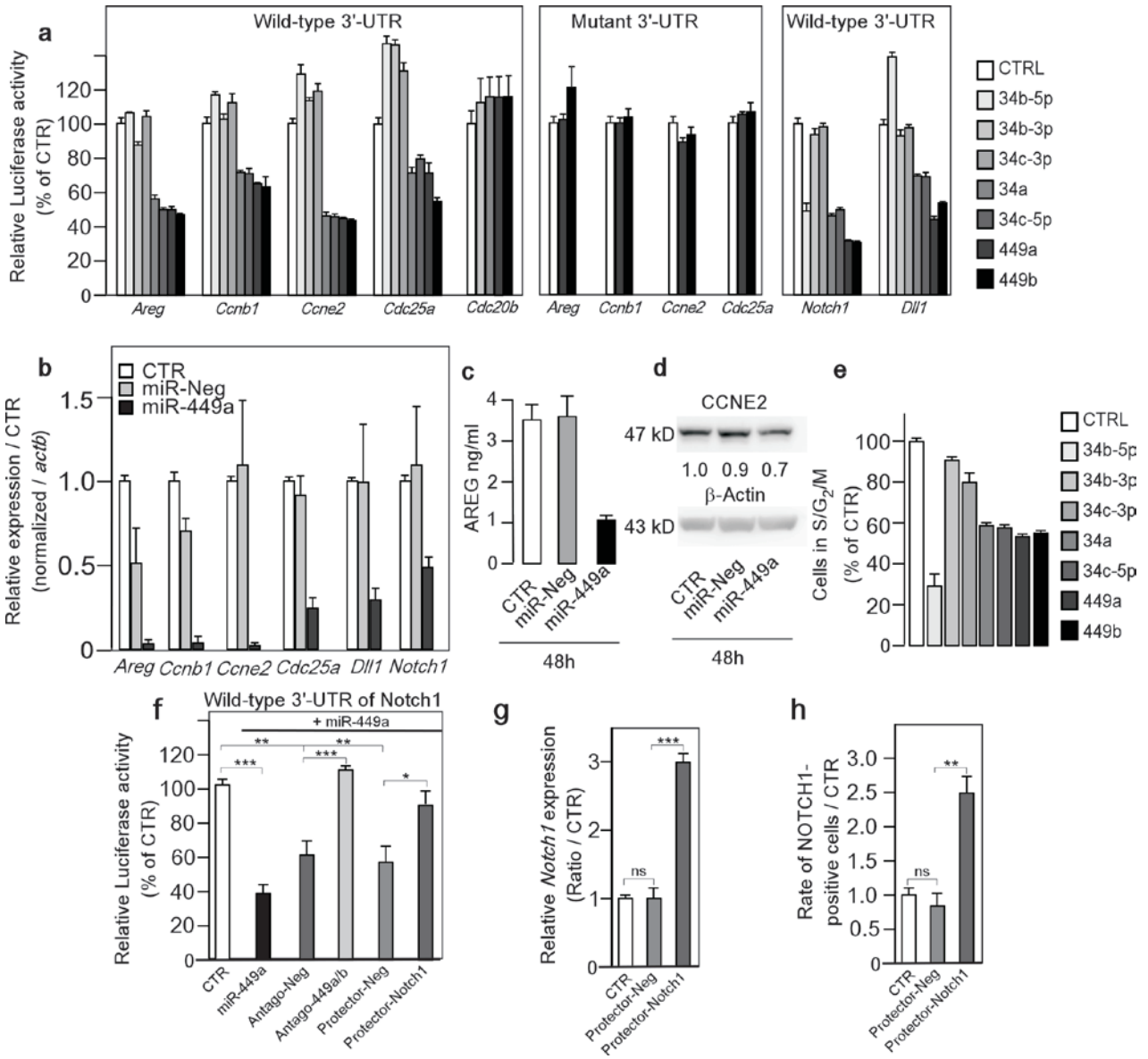

Figure S7 Repression by miR-449 of molecules related to cell cycle and to the Notch pathway. (a) A first group of validated miR-449a/b targets code for cell cycle-related proteins[19]: *Amphiregulin (Areg)*, an EGF receptor ligand, *Ccnb1*, *Ccne2*, and *Cdc25a*. A second group of targets code for NOTCH1 and its ligand DLL1 (see Fig. 4). Specific interaction between miR-449 or miR-34 and their 3'-UTRs was confirmed using luciferase reporter assay on constructs carrying either the wild-type or mutants 3'-UTR-binding site of miR-449. miR-34a, miR-34c-5p, miR-449a and miR-449b, sharing the same binding site region, reduced relative luciferase activity of wild-type 3'-UTR chimeric constructs with *Areg*, *Ccnb1*, *Ccne2* and *Cdc25a*. Those effects were abolished on the corresponding mutated 3'-UTR chimeric constructs. Values were normalized to the internal *Renilla* Luciferase control (n=5 independent experiments). miR-449 exert no regulation on its host gene *Cdc20b*. (b) miR-449 overexpression in proliferating HAECs strongly reduced *Areg*, *Ccnb1*, *Ccne2, Cdc25a, Dll1* and *Notch1* transcript levels in comparison to miR-Neg and untreated (CTR) conditions using real-time RT-PCR. Transcript levels were normalized using *β-actin* gene (*actb*) (n=3 measurements on two donors). (c) Inhibition of AREG release in proliferating HAECs by miR-449 overexpression (ELISA). AREG participates through EGF pathway to the induction of a mucus-producing airway epithelium[40] (n=3 measurements on two donors). (d) Inhibition of CCNE2 expression after miR-449 overexpression in proliferating HAECs (n=2 donors). (e) Cell cycle arrest in the G1 phase after transfection of A549 with synthetic miR-449 (n=3 measurements on two donors). (f) Antago-449a/b and *Notch1* protector oligonucleotide specifically prevent miR-449 binding on *Notch1* 3'UTR. miR-449a transfection in HEK293 cells strongly reduced relative luciferase activity of wild-type 3'-UTR chimeric constructs of *Notch1*. This effect was strongly blocked by antago-449a/b or *Notch1* protector co-transfection, whereas it was not significantly affected by co-transfection with negative controls (antago-Neg or protector-Neg). Values were normalized to the internal *Renilla* Luciferase control. (g-h) Validation of *Notch1* protection in HAECs. Chronic treatment of HAECs with *Notch1* protector oligonucleotide (20 nM) significantly increased *Notch1* transcript level in comparison to negative protector and untreated (CTR) conditions, as revealed by real-time RT-PCR (g), as well as the number of Notch1-positive HAECs relative to control (h). Transcript levels were normalized using *actb*. Error bars denotes standard deviation from five individual experiments (***, P<0.001; **, P<0.01; *, P<0.05, Student's *t-test*).

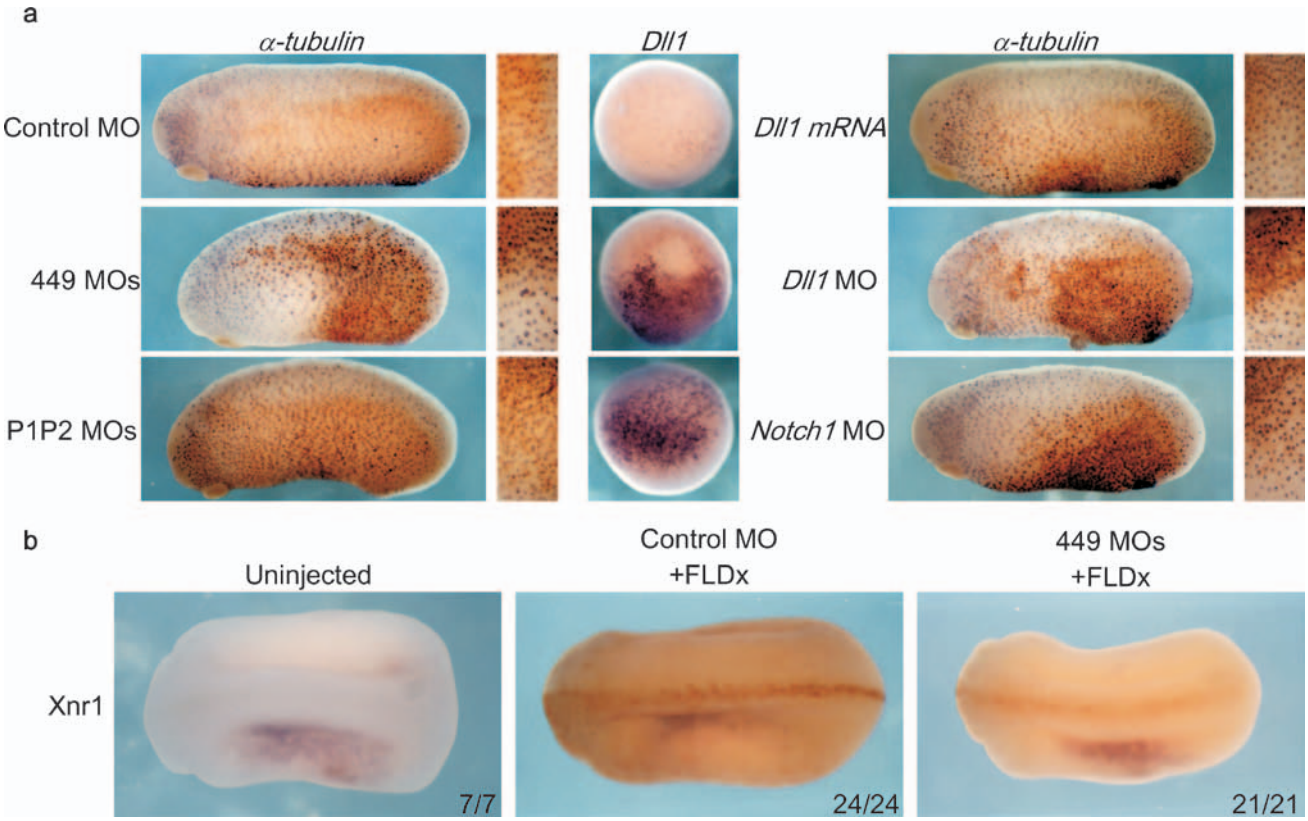

Figure S8 (a) Notch pathway modulation does not prevent ciliated cell specification. Cleavage stage embryos were injected in the epidermis with a mixture of anti miR-449 MOs, control MO, *Dll1* mRNA, *Dll1* MO, *Notch1* MO or *Dll1* protector P1P2 MOs, together with FLDx to trace injected cells. Note that in all cases, the density of ciliated cell progenitors marked by α-tubulin expression was increased in injected domains, indicating that cell specification is not blocked by any of these treatments. The excess number of ciliated cell progenitors can be explained by reduced lateral inhibition in the case of *Dll1* and *Notch1* MOs and by Notch cis-inhibition in cells exposed to injected *Dll1* mRNA or P1P2 MOs. This effect had been reported in Deblandre *et al* [25]. The expression of *Dll1* was also analysed in embryos injected with control, miR-449 and P1P2 MOs. Note that the lack of interaction between miR-449 and *Dll1* 3'-UTR caused the up-regulation of *Dll1* transcripts. **(b)** miR-449 knockdown does not affect left/right asymmetry. 4-cell embryos were injected with control or miR-449 MOs, together with FLDx (in brown) as a lineage tracer, in the marginal zone of the two dorsal cells. The targeted region gives rise to the gastrocoele roof plate, a territory covered with motile monociliated cells that is responsible to establish left/right asymmetry. *Xnr1* (the *Xenopus* counterpart to mammalian *nodal*) mRNA expression (revealed in blue), which is normally restricted to the left lateral plate mesoderm of tailbud embryos, is maintained in its normal site in miR-449 morphants (embryos are in dorsal view). The number of embryos showing normal *Xnr1* unilateral expression over the total number of embryos analysed is indicated (3 independent experiments).

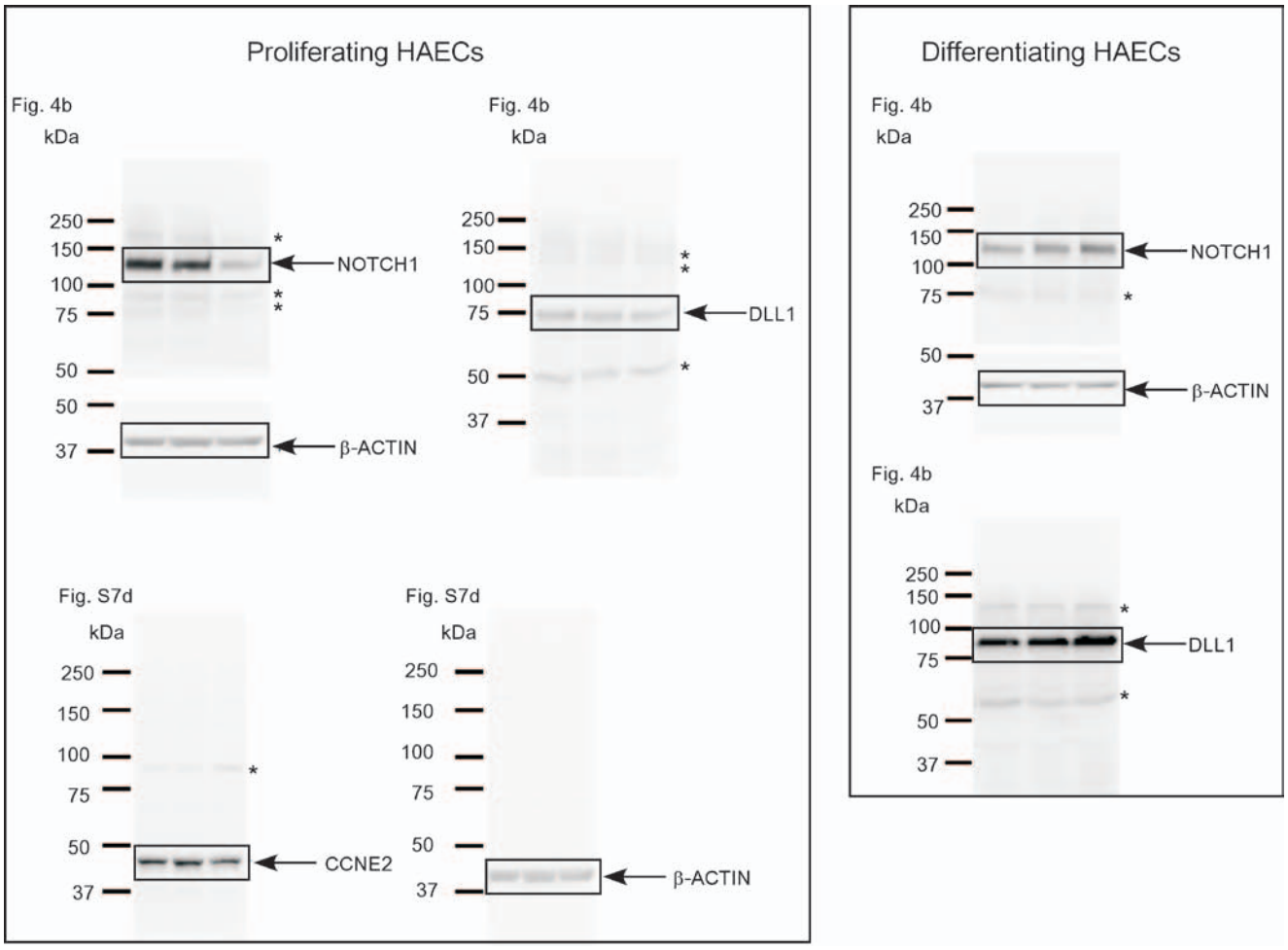

Figure S9 Full scans of western data. *Non-specific bands.

Table S1 Predicted members of the miRs-449 family. MicroRNAs located in syntenic region of *Cdc20b*. Sequence upstream to *Gpx8* gene was analyzed for the presence of the conserved seed sequence. The folded precursor structure was computed using the RNAfold program from the ViennaRNA suite. The stem-loop coordinates were retrieved using Ensembl Blat. (1) *Cdc20b* gene prediction. (2) Non-complete microRNAs stem-loop. Note that *Xenopus laevis* miR-449a shares an identical sequence with *Xenopus tropicalis*, as revealed by HTS experiments.

Species		ID	Status	Reference	Genome	Genomic coordinates	Host gene
Human	*Homo sapiens*	hsa-mir-449a	MiRbase	MI0001648	GRCh37	5:54466360-54466450 [-]	
		hsa-mir-449b	MiRbase	MI0003673	GRCh37	5:54466474-54466570 [-]	CDC20B
		hsa-mir-449c	MiRbase	MI0003823	GRCh37	5:54468090-54468181 [-]	
Chimpanzee	*Pan troglodytes*	ptr-mir-449a	MiRbase	MI0008670	PanTro2.1	5:60754105-60754194 [+]	
		ptr-mir-449b	MiRbase	MI0008671	PanTro2.1	5:60753985-60754080 [+]	CDC20B
		ptr-mir-449c	Predicted		PanTro2.1	5:60752369-60752472 [+]	
Macaque	*Macaca mulatta*	mml-mir-449a	MiRbase	MI0007747	MMUL1.0	6:52815640-52815730 [-]	
		mml-mir-449b	MiRbase	MI0007748	MMUL1.0	6:52815754-52815850 [-]	CDC20B
		mml-mir-449c	NA [3]		MMUL1.0	6:52817712-52817769 [-]	
Mouse	*Mus Musculus*	mmu-mir-449a	MiRbase	MI0001649	NCBIM37	13:113827742-113827832 [+]	
		mmu-mir-449b	MiRbase	MI0005547	NCBIM37	13:113827627-113827706 [+]	CDC20B
		mmu-mir-449c	MiRbase	MI0004645	NCBIM37	13:113826191-113826299 [+]	
Cow	*Bos taurus*	bta-mir-449a	MiRbase	MI0009834	BTAU4.0	20:25597468-25597555 [+]	
		bta-mir-449b	MiRbase	MI0009835	BTAU4.0	20:25597344-25597441 [+]	CDC20B
		bta-mir-449c	MiRbase	MI0009836	BTAU4.0	20:25595834-25595939 [+]	
Horse	*Equus caballus*	eca-mir-449a	Mirbase	MI0012851	EquCab2	21:17151965-17152024 [+]	
		eca-mir-449b	Predicted		EquCab2	21:17151831-17151915 [+]	CDC20B
		eca-mir-449c	Predicted		EquCab2	21:17150625-17150721 [+]	
Dog	*Canis familiaris*	cfa-mir-449a	MiRbase	MI0001651	BROADD2	2:45390354-45390444 [-]	CDC20B[2]
		cfa-mir-449b	Predicted		BROADD2	2:45390485-45390556 [-]	
Rat	*Rattus norvegicus*	rno-mir-449a	MiRbase	MI0001650	RGSC3.4	2:44418273-44418363 [+]	
		rno-mir-449b	Predicted		RGSC3.4	2:44418162-44418244 [+]	CDC20B[1]
		rno-mir-449c	Predicted		RGSC3.4	2:44416739-44416837 [+]	
Opossum	*Monodelphis domestica*	mdo-mir-449e	Predicted		MONDOM5	3:17544571-17544664 [-]	CDC20B[2]
		mdo-mir-449a	MiRbase	MI0005329	MONDOM5	3:17545606-17545684 [-]	
Platypus	*Ornithorhynchus anatinus*	oan-mir-449a	MiRbase	MI0006793	OANA5	Contig3432: 5911-6025 [+]	
		oan-mir-449b	MiRbase	MI0006792	OANA5	Contig3432: 5779-5880 [+]	CDC20B
		oan-mir-449c	MiRbase	MI0006791	OANA5	Contig3432: 4405-4521 [+]	
Chicken	*Gallus gallus*	gga-mir-449a	MiRbase	MI0003715	WASHUC2	Z:16040613-16040698 [-]	
		gga-mir-449b	MiRbase	MI0007566	WASHUC2	Z:16040763-16040856 [-]	CDC20B[2]
		gga-mir-449c	MiRbase	MI0007445	WASHUC2	Z:16041927-16041998 [-]	
Lizard	*Anolis carolinensis*	aca-mir-449e	Predicted		AnoCar1.0	282:1086809-1086891 [+]	
		aca-mir-449a	Predicted		AnoCar1.0	282:1086142-1086234 [+]	CDC20B[1,2]
		aca-mir-449c	Predicted		AnoCar1.0	282:1084259-1084350 [+]	
Xenopus	*Xenopus tropicalis*	xtr-mir-449a	MiRbase	MI0004957	JGI4.1	scaffold_715:164904-164990 [-]	
		xtr-mir-449b	Submitted	MI0018161	JGI4.1	scaffold_715:165047-165132 [-]	CDC20B[1]
		xtr-mir-449c	Submitted	MI0018162	JGI4.1	scaffold_715:165282-165374 [-]	
Stickleback	*Gasterosteus aculeatus*	gac-mir-449f	Predicted		BROADS1	groupXIII:2242237-2242322 [-]	
		gac-mir-449g	Predicted		BROADS1	groupXIII:2241856-2241935 [-]	CDC20B[1]
		gac-mir-449h	Predicted		BROADS1	groupXIII:2241594 2241676 [-]	
Medaka	*Oryzias latipes*	ola-mir-449g	Predicted		MEDAKA1	9:4531393-4531477 [+]	CDC20B[1]
		ola-mir-449h	Predicted		MEDAKA1	9:4531529-4531617 [+]	
Tetraodon	*Tetraodon nigroviridis*	tni-mir-449f	Predicted		TETRAODON8.0	12:5648354-5648441[+]	
		tni-mir-449g	Predicted		TETRAODON8.0	12:5648468-5648559[+]	CDC20B[1]
		tni-mir-449h	Predicted		TETRAODON8.0	12:5648615-5648697 [+]	
Fugu	*Takifugu rubripes*	fru-mir-449g	Predicted		FUGU4	scaffold_360:9120-9209 [-]	CDC20B[1]
		fru-mir-449h	Predicted		FUGU4	scaffold_360:8975-9057 [-]	